Impact of Intercontinental Pollution Transport on North American Ozone Air Pollution: An HTAP Phase 2 Multi-model Study

Min Huang[1,2], Gregory R. Carmichael[3], R. Bradley Pierce[4], Duseong S. Jo[5], Rokjin J. Park[5], Johannes Flemming[6], Louisa K. Emmons[7], Kevin W. Bowman[8], Daven K. Henze[9], Yanko Davila[9], Kengo Sudo[10], Jan Eiof Jonson[11], Marianne Tronstad Lund[12], Greet Janssens-Maenhout[13], Frank J. Dentener[13], Terry J. Keating[14], Hilke Oetjen[8,*], Vivienne H. Payne[8]

[1]George Mason University, Fairfax, VA, USA
[2]University of Maryland, College Park, MD, USA
[3]University of Iowa, Iowa City, IA, USA
[4]NOAA National Environmental Satellite, Data, and Information Service, Madison, WI, USA
[5]Seoul National University, Seoul, Korea
[6]European Center for Medium range Weather Forecasting, Reading, UK
[7]National Center for Atmospheric Research, Boulder, CO, USA
[8]Jet Propulsion Laboratory, California Institute of Technology, Pasadena, CA, USA
[9]University of Colorado-Boulder, Boulder, CO, USA
[10]Nagoya University, Furocho, Chigusa-ku, Nagoya, Japan
[11]Norwegian Meteorological Institute, Oslo, Norway
[12]Center for International Climate and Environmental Research, Oslo, Norway
[13]European Commission, Joint Research Center, Ispra, Italy
[14]US Environmental Protection Agency, Washington, DC, USA
[*]Now at: University of Leicester, Leicester, UK

Correspondence to: Min Huang (mhuang10@gmu.edu)

Abstract

The recent update on the US National Ambient Air Quality Standards of the ground-level ozone (O_3) can benefit from a better understanding of its source contributions in different US regions during recent years. In the Hemispheric Transport of Air Pollution experiment Phase 1 (HTAP1), various global models were used to determine the O_3 source-receptor relationships among three continents in the Northern Hemisphere in 2001. In support of the HTAP Phase 2 (HTAP2) experiment that studies more recent years and involves higher-resolution global models and regional models' participation, we conduct a number of regional scale Sulfur Transport and dEposition Model (STEM) air quality base and sensitivity simulations over North America during May-June 2010. STEM's top and lateral chemical boundary conditions were downscaled from three global chemical transport models' (i.e., GEOS-Chem, RAQMS, and ECMWF C-IFS) base and sensitivity simulations in which the East Asian (EAS) anthropogenic emissions were reduced by 20%. The mean differences between STEM surface O_3 sensitivities to the emission changes and its corresponding boundary condition model's are smaller than those among its boundary condition models, in terms of the regional/period mean (<10%) and the spatial distributions. An additional STEM simulation was performed in which the boundary conditions were downscaled from a RAQMS simulation without EAS anthropogenic emissions. The scalability of O_3 sensitivities to the size of the emission perturbation is spatially varying, and the full source contribution obtained by linearly scaling the North American mean O_3 sensitivities to a 20% reduction in the EAS anthropogenic emissions may be underestimated by at least 10%.

The three boundary condition models' mean O_3 sensitivities are ~8% (May-June 2010)/~11% (2010 annual) lower than those estimated by multiple global models, and the multi-model ensemble estimates are higher than the HTAP1 reported 2001 conditions, due to the growing EAS anthropogenic emissions, the interannual variability in atmospheric circulation (i.e., stronger trans-Pacific transport in spring 2010 following an El Niño event), and the different experiment designs of HTAP1 and HTAP2. GEOS-Chem sensitivities indicate that the EAS anthropogenic NO_x emissions matter more than the other EAS O_3 precursors to the North American O_3, qualitatively consistent with previous adjoint sensitivity calculations.

In addition to the analyses on large spatial/temporal scales relative to the HTAP1, we also show results on subcontinental- and event-scale that are more relevant to the US air quality management. Satellite O_3 (TES, JPL-IASI, and AIRS) and carbon monoxide (TES and AIRS) products, along with surface measurements and model calculations, show that during certain episodes stratospheric O_3 intrusions and the transported EAS pollution influenced O_3 in the western and the eastern US differently. Free-running global models underpredicted the transported background O_3 during these episodes, posing difficulties for STEM to accurately simulate the surface O_3 and its source contribution. Although we effectively improved the modeled O_3 by incorporating satellite O_3 (OMI and MLS) and evaluated the quality of the HTAP2 emission inventory with the KNMI OMI nitrogen dioxide, using observations to evaluate and improve O_3 source attribution still remains to be further explored.

1. Introduction

Tropospheric ozone (O_3), a short-lived trace gas with a lifetime ranging from hours in the boundary layer to weeks in the free troposphere, affects tropospheric chemistry, harms human and ecosystem health, and induces climate change on local, regional and global scales (Jerrett et al., 2009; Smith et al., 2009; Anenberg et al., 2010; Mauzerall and Wang, 2001; Avnery et al., 2011a, b; Shindell et al., 2009, 2013; Bowman and Henze, 2012; Stevenson et al., 2006, 2013; Monks et al., 2015). It has been recognized that the uneven distributions of tropospheric O_3 can be attributed to the stratosphere as well as local, regional and distant emission sources, through complicated processes that occur on synoptic, meso- and micro-scales (Task Force on Hemispheric Transport of Air Pollution (HTAP), 2010; National Research Council (NRC), 2009; Maas and Grennfelt, 2016). The mitigation of O_3's climate and health impacts would benefit from efforts to control the emissions of its precursors from the various emission sources (United Nations Environment Programme (UNEP) and World Meteorological Organization (WMO), 2011), such as nitrogen oxides (NO_x), carbon monoxide (CO), methane (CH_4), and non-methane volatile organic compounds (NMVOCs).

Ground-level O_3 is one of the six criteria air pollutants regulated by the US Environmental Protection Agency (EPA), and the US National Ambient Air Quality Standards (NAAQS) has recently been lowered to 70 ppbv to better protect Americans' health and the environment. Issues regarding making accurate estimates of the total O_3 as well as the background O_3 level (defined as the concentration that is not affected by recent locally-emitted or produced anthropogenic pollution) (e.g., McDonald-Buller et al., 2011; Zhang et al., 2011; Fiore et al., 2014; Huang et al., 2015), have been recently discussed as part of the implementation of the new US O_3 standard (US EPA, 2016a, b). This includes assessing the impacts of various components of the background O_3, such as stratospheric O_3, local natural sources such as biogenic, lightning and wildfire emissions, as well as the long-range transport (LRT) of pollution. The impact of the trans-Pacific pollution transport on US air quality has been evaluated in numerous studies over the past decades (e.g., Fiore et al., 2009; Reidmiller et al., 2009; Zhang et al., 2008, 2009; Huang et al., 2010, 2013a; Lin et al., 2012a, 2015, 2016; US EPA, 2016a). It has been found that the increasing trends of pollution in the upwind continents, especially the populated East Asia (e.g., Zhang et al., 2014; Susaya et al., 2013; Wang et al., 2012), may partially offset the US air quality improvements in recent decades due to the regional and local emission controls (e.g., Jacob et al., 1999; Verstraeten et al., 2015; Ambrose et al., 2011; Wigder et al., 2013; Cooper et al., 2010; Parrish et al., 2009, 2012; Gratz et al., 2014). A better understanding of the processes that determine the O_3 pollution levels, as well as an improved capability of attributing the air pollution to nearby or distant sources is needed to assist with designing and implementing effective local emission control strategies to comply with the tighter air quality standards.

Chemical transport models are often used to reproduce and attribute the observed O_3 levels, including assessing the impacts of the internationally transported O_3 on the US air quality. In the HTAP modeling experiment Phase 1 (HTAP1), various global models with horizontal resolutions ranging from 1°×1° to 5°×5°, only around half of which are finer than 3°×3°, were used to determine the O_3 source-receptor (SR) relationships among three continents in the Northern Hemisphere in 2001 (Chapter 4 in HTAP, 2010). The global model based SR relationships in HTAP1 determined using the emission perturbation approach (i.e., calculating the changes of O_3

at the receptor regions in response to a 20% reduction in the emission inputs in a given source region) were reported as either monthly 24h mean values or policy-relevant metrics such as the maximum daily 8h average (MDA8) for the US (e.g., Fiore et al., 2009; Reidmiller et al., 2009). Large intermodel diversity was found in the simulated total O_3 and the intercontinentally transported pollution for the chosen SR pairs in the northern midlatitudes, indicating the challenges with model simulations to accurately represent the key atmospheric processes. Multi-model mean results were the foci of in these studies with the assumption that this approach can reduce the uncertainty from the single model estimates for monthly or seasonal means. "Ensemble" model analyses have been suggested by some US stakeholders as one of the methods for helping with the characterization of the background O_3 components (US EPA, 2016b). Although the multi-model approach can help identify some of the weaknesses of the individual models and may produce more reliable estimates, it is necessary to well understand the uncertainties inherent in using the same set of anthropogenic emissions in all these model simulations. Satellite observations over the regions with limited in-situ measurements such as the East Asia can be particularly helpful for quantifying such uncertainties.

The 20% emission perturbation in the HTAP1 modeling experiment was chosen to produce a sizeable (i.e., larger than numerical noise) and realistic impact, but small enough in the assumed near-linear atmospheric chemistry regime. The scalability of the modeled O_3 sensitivities to the size of the emission perturbations has been assessed on continental scale (Wu et al., 2009; Fiore et al., 2009; HTAP, 2010; Wild et al., 2012; Emmons et al., 2012). The receptor O_3 responses to the source-region emission perturbations are found to be fairly linear within ~50% of the perturbations. However, due to the chemical non-linearity, the full source contribution obtained by linearly scaling the receptor regional mean O_3 sensitivity to the 20% reduction in the source region emissions may be underestimated, and the scalability depended on seasons and the perturbed emission species. Huang et al. (2013b) investigated the scalability of the O_3 sensitivity between the southern California-US intermountain west SR pair for May 2010, in which study the southern California anthropogenic emissions were perturbed by multiple amounts of +50%, -50%, -100%. They reported that the scalability of the O_3 sensitivities changed with the distance from the source regions. Further analyses on the scalability of these modeled O_3 sensitivities during recent years especially for the East Asia-NAM SR pair, as well as their spatial variability, are still needed. Furthermore, results generated using the emission perturbation approach need to be compared with those based on the other methods (e.g., tagged tracers, adjoint sensitivity).

Previous studies have demonstrated the advantages of high resolution chemical transport modeling for understanding SR relationships (e.g., Lin et al., 2010 for Europe and the East Asia; Lin et al., 2012a; Huang et al., 2010, 2013a for Asia and NAM). Using observations (satellite, sondes, aircraft) along with single model simulations, a few studies have reported that the US O_3 sensitivities to extra-regional sources is time- and region-dependent (e.g., Lin et al., 2012a, b; Langford et al., 2011; Ott et al., 2016), and therefore the necessity of evaluating the extra-regional source impacts on event scale has been emphasized in these studies as well as in US EPA (2016a, b). The HTAP Phase 2 (HTAP2) multi-model experiment, initiated in 2012, is designed to advance the understanding of the impact of intercontinental pollution transport during more recent years (i.e., 2008-2010) involving a number of global and regional models' participation (Galmarini et al., 2017; Koffi et al., 2016). The regional models are anticipated to help connect the analyses over global and regional scales and enable discussions on small spatial (e.g., subcontinental) and

temporal scales (i.e., event based analyses). The use of satellite products for identifying the transport events as well as for quantitative model evaluation is also encouraged in the work plan. The HTAP2 modeling experiment was sequentially conducted in two steps. First, similar to the HTAP1 experiment, a group of global models with different resolutions conducted base and emission perturbation sensitivity simulations to determine the pollutants' SR relationships. All models in their base simulations used the same set of harmonized sector-based global anthropogenic emissions developed specifically for the HTAP2 modeling experiment (Janssens-Maenhout et al., 2015). Most of these global models recorded only key chemical species from their base and sensitivity simulations in varied temporal frequencies. Several global models saved the three-dimensional (3D) chemical fields of more species with a 3- or 6-hour interval, which are suitable for being used as regional models' chemical boundary conditions. In the second step, regional models conducted base and sensitivity simulations to analyze the pollutants' SR relationships in greater detail. The regional model simulations used the same set of anthropogenic emissions as the global models within their simulation domains, and the chemical boundary conditions in these regional simulations were downscaled from the base and sensitivity simulations from the selected boundary condition model outputs. For regional simulations over the North America and Europe, boundary conditions were mostly taken from a single model such as the ECMWF C-IFS or GEOS-Chem.

This study aims to address: 1) the differences in O_3 sensitivities generated from the HTAP2 and HTAP1 experiments to help address how the LRT impacts on NAM changed through time; 2) how the refined modeling experiment design in HTAP2 can help advance our understanding of the LRT impacts on NAM, particularly the involvement of regional models and the inclusion of small spatial/temporal scale analysis during high O_3 episodes that are more relevant to air quality management; 3) the usefulness of satellite observations for better understanding the sources of uncertainties in the modeled total O_3 (e.g., from the emission and regional models' boundary condition inputs) as well as for reducing the uncertainties in some of these model inputs via chemical data assimilation. We performed a number of regional scale STEM (Sulfur Transport and dEposition Model) base and sensitivity simulations over the NAM during May-June 2010, during which period strong trans-Pacific pollution transport were shown to episodically impact the US (Lin et al., 2012a). Extending the HTAP2 regional simulations' basic setup, the STEM top and lateral chemical boundary conditions were downscaled from three global models' (i.e., the Seoul National University (SNU) GEOS-Chem, RAQMS, and the ECMWF C-IFS) base and sensitivity simulations in which the East Asian anthropogenic emissions were reduced. The STEM surface O_3 sensitivities over the NAM region based on different boundary condition models were inter-compared, in terms of the regional averages and the spatial patterns on monthly basis and during a selected event identified by satellite O_3 and CO products. These were also compared with the sensitivities estimated by their corresponding boundary condition models as well as all HTAP2 participating global models and the results from HTAP1.

2. Methods

2.1. Anthropogenic emission inputs

Identical anthropogenic emissions were used in all global and regional chemical transport models' base and sensitivity simulations. This monthly-varying harmonized sectoral (i.e., power, industry, transportation, residential, shipping, aircraft, agriculture) emission inventory was

provided on a gridded 0.1°×0.1° resolution for the years of 2008 and 2010, by compiling the officially reported emissions at the national scale (Janssens-Maenhout et al., 2015; http://edgar.jrc.ec.europa.eu/htap_v2). The temporal profiles for developing the monthly-varying emissions differ by region and sector. The amount of emissions of key O_3 precursors (CO, NO_x, NMVOCs) from both years are summarized in Table S1 for the four major emissions sectors, over the NAM (US+Canada, based on data from the US EPA and the Environmental Canada, which shows lower emissions from the previous years as also discussed in Pouliot et al., 2015), MICS-Asia regions (south, southeast, and east Asia, based on country inventory for China and from the Clean Air Policy Support System and the Regional Emission inventory in ASia 2.1, more information also in Li et al., 2017), and for over the world. For all of these species, global total emissions in 2008 and 2010 are similar. The NO_x, NMVOC, and CO emissions decreased from 2008 to 2010 over the NAM by 10.7%, 9.4%, and 15.7%, respectively. In 2008, NAM NO_x, NMVOC and CO contributed to 18.0%, 11.7% and 11.9% of the global total, respectively, and in 2010, these contributions became 15.8%, 10.5% and 10.2%. For 2010, the transportation sector contributed more than the other sectors to NAM anthropogenic NO_x and CO emissions; industrial sector contributed more than the other sectors to NMVOCs emissions. Over East Asian countries, these emissions are ~2-5 times higher than the US emissions, and the NO_x, NMVOC and CO emissions increased over Asia by 7.3%, 7.2% and 1.0%, with the dominant emission sectors in 2010 of transportation, industry, and residential, respectively. For both years, the emissions over the MICS-Asia regions contribute to over 40% of the global emissions. For these key O_3 precursors, the East Asian countries contribute to 45% (NMVOCs)-70% (NO_x) of the emissions in the MICS-Asia domain in both years, and the south Asian countries contribute to ~22% (NO_x)-34% (NMVOCs) of the MICS-Asia emissions. The uncertainty of the emission estimates differs by emission sector and species: i.e., the emissions from large-scale combustion sources (e.g., NO_x and CO from power and industry sectors) are less uncertain than those from small-scale and scattered sources (e.g., CO and NMVOCs from transportation and residential sources). Non-anthropogenic emission inputs used in different models' simulations may differ, and their impacts on the modeled total O_3 and the SR relationships will be compared in detail in future studies.

2.2. Region definitions for the SR study and the model base and sensitivity simulations

2.2.1. Base and 20% emission perturbation simulations from global and regional models

The HTAP2 simulations from eight global models, used in this study, are listed in Table 1a, including the relevant references. Horizontal and vertical resolutions of these models range from finer than 1° to coarser than 2.5°, and from 20 to 60 layers, respectively. Overall these resolutions are higher than the HTAP1 participating models'. Figure 1 defines the source regions used in the HTAP2 SR relationship study and we will focus in this study on assessing the East Asia (EAS), S Asia (SAS), Europe (EUR), and non-NAM anthropogenic source (interchangeable in this paper with "(all) foreign") impacts on the NAM O_3 levels in 2010. Specifically, each model performed a base simulation and a number of sensitivity simulations in which the original HTAP2 anthropogenic emissions for all species and sectors in a defined source region were perturbed by a certain amount (referring to 20% as in most cases) and these cases are defined in Table 1a-b as **source region**ALL(**perturbation**), where "ALL" refers to "all species and sectors", consistent with HTAP1 and HTAP2's naming convention. The O_3 differences R(O_3, **source region**, **perturbation**) over the NAM were then calculated between each model's base and sensitivity simulations:

$R(O_3, EAS, 20\%) = BASE\ O_3 - EASALL(-20\%)\ O_3$ (1a)

$R(O_3, SAS, 20\%) = BASE\ O_3 - SASALL(-20\%)\ O_3$ (1b)

$R(O_3, EUR, 20\%) = BASE\ O_3 - EURALL(-20\%)\ O_3$ (1c)

$R(O_3, non\text{-}NAM, 20\%) = NAMALL\ O_3 - GLOALL(-20\%)\ O_3$ (1d)

The monthly-mean $R(O_3,$ **source region**, 20%) values were averaged over the NAM region for the analysis and compared with the findings in the HTAP1 study (e.g., Fiore et al., 2009). It is worth mentioning that the rectangular source regions defined in HTAP1 were modified in HTAP2 to align with the geo-political borders. For EAS and SAS, the regions not overlapped by HTAP1 and HTAP2 are mostly in the less populated/polluted regions such as the northwestern China, according to the HTAP2 emission maps (http://edgar.jrc.ec.europa.eu/htap_v2/index.php). HTAP2's EUR domain excludes certain regions in Russia/Belarussia/Ukraine, Middle East and North Africa that are included in HTAP1's EUR domain. The impact of emissions over these regions on comparing the NAM $R(O_3, EUR, 20\%)$ values in HTAP1 and HTAP2 will be discussed in Section 3.2.1.

A unitless "Response to Extra-Regional Emission Reductions (RERER)" metric (Galmarini et al., 2017), as defined in eq. (2), was also calculated to measure the importance of local versus non-local sources to NAM's O_3 levels:

$$RERER\ (O_3, NAM) = \frac{R_{O3,non-NAM,20\%}}{R_{O3,global,20\%}} = \frac{(NAMALL\ O3 - GLOALL\ O3)}{(BASE\ O3 - GLOALL\ O3)} \quad (2)$$

The denominator and numerator terms of RERER represent the impacts of global and non-NAM anthropogenic emissions on NAM O_3, respectively. The higher the NAM RERER value is, the stronger impact from non-local sources on NAM is indicated. The RERER value can exceed 1, when emission reductions led to increasing concentrations (e.g. O_3 titration by nitrogen monoxide (NO)).

The STEM (version 2K3) regional simulations were then performed on a 60 km×60 km horizontal resolution (a typical coarse regional model resolution) grid over NAM within the domain defined in Figure 2a during May-June 2010. The meteorological conditions in spring 2010 were compared with the climatology from the NCEP/NCAR reanalysis data for the 1981-2010 period (Kalnay et al., 1996) in Huang et al. (2013b), concluding that this spring represents a period of stronger-than-climatological average spring trans-Pacific transport, based on a stronger meridional gradient in the North Pacific and higher Pacific/North American (PNA) indexes. This is consistent with the findings by Lin et al. (2014) that the El Niño conditions during the 09/10 winter strengthened the trans-Pacific transport of Asian pollution in spring 2010. The mean near-surface air temperatures in the western US in this spring were lower than the climatology, with larger anomalies in the mountain states, which may have led to weaker local O_3 production and decomposition of the transported peroxyacyl nitrates (PAN). In contrast, higher-than-normal temperatures were found in the eastern US that favored anomalously strong local O_3 production.

STEM has been used to interpret the observations collected by satellites and during aircraft campaigns in the past decade (e.g., Carmichael et al., 2003a, b; Huang et al., 2010, 2013a, b, 2014, 2015). STEM calculates gas-phase chemistry reactions based on the SAPRC 99 gaseous chemical mechanism (Carter, 2000) with thirty photolysis rates calculated online by the Tropospheric Ultraviolet-Visible radiation model (Madronich et al., 2002). Most of the key configurations of the 60 km base simulations are the same as those described in Lapina et al. (2014), i.e., meteorological

fields were pre-calculated by the Advanced Research Weather Research and Forecasting Model (WRF-ARW, Skamarock et al., 2008) version 3.3.1 forced by the North American Regional Reanalysis data (Mesinger et al., 2006), using a similar set of the physics configuration to those in Huang et al. (2013a). Biomass burning emissions are from the Fire INventory from NCAR (FINN) inventory version 1.0 (Wiedinmyer et al., 2011). Biogenic emissions were calculated by the Model of Emissions of Gases and Aerosols from Nature (MEGAN) version 2.1 (Guenther et al., 2012), driven by the WRF meteorology. Lightning NO_x emissions are generated following the method in Allen et al. (2012), with the flash rates determined by the WRF convective precipitation and scaled to the National Lightning Detection Network flash rates. A major difference of the STEM simulations in this study from the Lapina (2014) study is that the anthropogenic emissions were replaced with the monthly-mean HTAP2 inventory with no weekday-weekend variability applied, rather than the earlier National Emission Inventory (NEI) 2005 in which the weekday-weekend variability exists. This change can introduce uncertainty for some US regions where weekday-weekend variability of some O_3 precursors' emissions was notable during the studied period (e.g., weekend NO_x emissions in southern California during spring/summer 2010 were 0.6-0.7 of the weekday emissions as reported by Kim et al. (2016) and Brioude et al. (2013)), but this was done to ensure consistency with the HTAP2 global model simulations, that also didn't use daily variable emissions for any regions in the world. The VOC speciation for the SPRAC 99 chemical mechanism in the NEI 2005 (ftp://aftp.fsl.noaa.gov/divisions/taq/emissions_data_2005) were applied to break down the total NMVOC emissions provided in the HTAP2 inventory. The VOC speciation based on the year of 2005 can be unrealistic for 2005 as well as 2010 as studies have reported variable temporal changes of different VOC species in some US cities (e.g., Warneke et al., 2012). The time-varying lateral and top boundary conditions in the STEM base simulations were downscaled from three global models (i.e., 3 hourly SNU GEOS-Chem, 3 hourly ECMWF C-IFS, and 6 hourly RAQMS) base simulations. In support of the SR relationship study to quantify the East Asia anthropogenic impacts on the NAM, three STEM sensitivity simulations were also conducted in which the STEM boundary conditions were downscaled from the EASALL(-20%) sensitivity simulations by these three global models (Table 1b). All STEM simulated 3D chemical fields were saved hourly for the convenience of calculating the US primary O_3 standard metric MDA8 as well as the quantitative comparisons against the satellite Level 2 (L2) O_3 products. The STEM base case surface O_3 performance and its O_3 sensitivities were also compared with those of its boundary condition models as well as the multi- global model means. The latitude/longitude ranges (20-50°N/130-65°W) of NAM for the global and regional model based sensitivity calculations were selected to mainly account for the coverage of the STEM domain, which are slightly different from the definition of North America in HTAP1.

Note that non-anthropogenic emission inputs used in STEM and its boundary condition models differed, as summarized in Table 1c. Figure S1 shows detailed comparisons between STEM and GEOS-Chem's non-anthropogenic (i.e., soil, lightning, biomass burning) NO_x emission inputs, and their impacts on the modeled NAM background O_3 were included in Lapina et al. (2014). Such quantitative comparisons will also be carried out between STEM and its other boundary condition models in future studies.

2.2.2. Additional base and sensitivity simulations from selected models

In addition to the base and 20% EAS all-category emission perturbation simulations, the global RAQMS model conducted a sensitivity simulation in which the East Asian anthropogenic emissions were zeroed out, which was also used as STEM's boundary conditions (Table 1b). We calculate the "S_{O3}" metric (eq. (3)) using the O_3 sensitivities in STEM and RAQMS at the receptor regions in response to both 20% and 100% of emission reductions, to explore the relationships between the O_3 sensitivity and the size of the emission perturbation. A closer-to-one "S_{O3}" value indicates higher scalability of the sensitivity based on the 20% emission perturbation method for obtaining the full "contribution" of the East Asian anthropogenic emissions on the NAM O_3.

$$S_{O3} = R(O_3, EAS, 100\%)/R(O_3, EAS, 20\%)/5 \quad (3)$$

Where: $R(O_3, EAS, 100\%) = BASE\ O_3 - EASALL(-100\%)\ O_3$

The RAQMS model also provided a base simulation that assimilated satellite O_3 products from the Ozone Monitoring Instrument (OMI, Levelt et al., 2006) and Microwave Limb Sounder (MLS, Livesey et al., 2008) (Pierce et al., 2007), which was used to help better understand the regional model base run error sources, as well as for demonstrating the use of satellite observations to help improve the representation of the trans-boundary pollution.

We also used a number of sensitivity simulations produced by the GEOS-Chem adjoint model v35f in which the emissions from selected anthropogenic emission sectors (power&industry, transportation, residential) or individual O_3 precursor chemical species (NO_x, VOC, CO) over the East Asia were reduced by 20%. Additional simulations for the 2008-2009 periods by the SNU GEOS-Chem were also utilized to quantify the East Asia and non-NAM anthropogenic source impacts in comparison with the 2010 conditions that we mainly focus on in this study.

2.3. In-situ and satellite observations

2.3.1. In-situ observations

Over the receptor NAM, the hourly O_3 observations at the Clean Air Status and Trends Network (CASTNET, http://epa.gov/castnet/javaweb/index.html) sites were used to evaluate the global and regional models' base simulations in four subregions: western US (i.e., the EPA regions 8, 9, 10); southern US (i.e., the EPA regions 4 and 6), the Midwest (i.e., the EPA regions 5 and 7), and the northeast (i.e., the EPA regions 1-3). The numbers of sites used in global and regional models' evaluation in each US subregion are summarized in Tables 2-3. The locations of these sites and the subregions they belong to are indicated in Figure 2a, overlaid on a model-based terrain height map. A majority of the CASTNET sites in the western US are located at high elevation (>1 km) remote or rural regions, more susceptible to the trans-boundary pollution (e.g., Jaffe, 2011). Most of the sites in the other three subregions are located in low elevation regions, mainly affected by local and regional pollution. The model-based terrain heights fairly well represent the reality on subregional scale – the differences between the actual and model-based subregional mean terrain heights at the CASTNET sites are smaller than 0.1 km (Table 3).

During May-June 2010, intense ozonesonde measurements were made at multiple California locations (Cooper et al., 2011), in support of the NOAA "California Nexus (CalNex): Research at the Nexus of Air Quality and Climate Change" field experiment (Ryerson et al., 2013). They have been used to evaluate the simulated O_3 vertical profiles by the HTAP2 participating models. The detailed evaluation results have been shown by Cooper et al. (2016), and will be covered by subsequent publications.

Over HTAP2's EAS source region, the global models' O_3 performance was evaluated against the monthly-mean surface in-situ O_3 measurements at 11 sites within the Acid Deposition Monitoring Network in East Asia (EANET, http://www.eanet.asia) that had data throughout the year of 2010. These include eight Japanese and three Korean sites (Figure 3a), all of which are located at low elevation regions (2-150 m). The reported monthly mean observations at these sites were based on weekly or daily sampled data, varying among sites.

2.3.2. Satellite products

In two case studies of high O_3 episodes, L2 and L3 O_3 and CO retrievals from several satellite instruments were used to assess the impacts of trans-Pacific pollution transport and stratospheric O_3 intrusions on NAM O_3 levels in early May. These include: 1) the early afternoon O_3 and CO profiles version 5 from the Tropospheric Emission Spectrometer (TES) (Beer et al., 2001; Beer, 2006) on the Aura satellite; 2) the mid-morning O_3 profiles from the METOP-Infrared Atmospheric Sounding Interferometer (IASI), which were retrieved using the Jet Propulsion Laboratory (JPL) TES optimal estimation retrieval algorithm (Bowman et al., 2006) for selected areas including the western US (Oetjen et al., 2014, 2016); as well as 3) the early afternoon L3 O_3 and CO maps (version 6, 1°×1°) from the Aqua Atmospheric Infrared Sounder (AIRS) instrument. The TES tropospheric O_3 retrieval is often sensitive to the mid- to lower free troposphere, and O_3 at these altitudes in the Eastern Pacific is known to possibly impact the downwind US surface air quality at later times (Huang et al., 2010; Parrish et al., 2010). TES O_3 is generally positively biased by <15% relative to high accuracy/precision reference datasets (e.g., Verstraeten et al., 2013). Although IASI is in general less sensitive than TES due to its coarse spectral resolution, the 681–316 hPa partial column-averaged O_3 mixing ratios in the JPL product agree well with TES O_3 for the 2008–2011 period with a -3.9 ppbv offset (Oetjen et al., 2016). Note that IASI O_3 data are processed operationally in Europe using a different algorithm. For this work we used O_3 profiles from TES and IASI processed using a consistent algorithm at JPL, although the latter set of data represents only a small subset of the full set of the IASI radiance measurements. The IASI and TES L2 O_3 profiles (screened by the retrieval quality and the C-Curve flags) were used to evaluate the STEM O_3 vertical distributions in the different base simulations, and the satellite observation operators were applied in these comparisons. Taking TES as an example, its observation operator h_z for O_3 is written in (4):

$$h_z = z_c + \mathrm{A_{TES}}\ (\ln(F_{TES}(c)) - z_c) \quad (4)$$

where z_c is the natural log form of the TES constraint vector (a priori) in volume mixing ratio. A_{TES} is the averaging kernel matrix reflecting the sensitivity of retrieval to changes in the true state (Rodgers, 2000). F_{TES} projects the modeled O_3 concentration fields c to the TES grid using spatial and temporal interpolation. The exponential of h_z is then used to compute the mismatches between the model and TES O_3 retrievals as the model evaluation. A small mismatch between model with the satellite observation operators and the satellite retrievals may indicate either good model performance or may be the low sensitivity of the retrievals to the true O_3 profile. AIRS O_3 is sensitive to the altitudes near the tropopause, with positive biases over the ozonesondes in the upper troposphere (e.g., Bian et al., 2007); AIRS CO is most sensitive to 300–600 hPa (Warner et al., 2007) and is frequently used together with the AIRS O_3 to distinguish the stratospheric O_3 intrusions from long-range transported anthropogenic or biomass burning pollution. We use the L3 AIRS products in this study to get a broad overview of the areas that are strongly impacted by the stratospheric O_3 intrusions or/and LRT of pollution.

The bottom-up NO_x emissions from the HTAP2 inventory were assessed on a monthly base by comparing the GEOS-Chem nitrogen dioxide (NO_2) columns with the de-striped KNMI (Royal Netherlands Meteorological Institute) OMI column NO_2 product version 2.0 (Boersma et al., 2011a, b). For this model evaluation against the OMI L2 products, the NO_2 fields calculated by the GEOS-Chem adjoint model were saved daily at 13:30 local solar time, roughly coinciding with the Aura and Aqua overpassing times. Other parameters used in the model column calculations came from the GEOS-5/GEOS-Chem monthly mean conditions. The OMI data that passed the tropospheric quality flag at 13-14 local time were selected based on the following screening criteria: surface albedo<0.3; cloud fraction<0.2; solar zenith angle <75°; and viewing zenith angle <45°. The averaging kernels (Eskes and Boersma, 2003) and Air Mass Factors (AMFs) in the KNMI product were used to calculate the modeled tropospheric NO_2 vertical columns comparable to the OMI's. Details of the method to compare the model-based NO_2 columns with the KNMI OMI's can be found in Huang et al. (2014).

3. Results and Discussions

3.1. Evaluation of the HTAP2 bottom-up NO_x emissions and the model base simulations

3.1.1. Evaluation of the bottom-up NO_x emissions

The comparison of the GEOS-Chem adjoint NO_2 columns with the OMI product was used to help assess the bottom-up HTAP2 NO_x emissions. Figure 4 shows that NO_2 columns from GEOS-Chem's base simulations over the US are overall overestimated. While grid-scale differences in NO_2 columns may not be directly indicative of emissions biases (Qu et al., 2016), these discrepancies are possibly due to a positive bias in the bottom-up emissions, mainly from the anthropogenic sources, which have also been pointed out by Anderson et al. (2014) and Travis et al. (2016). Larger OMI-model disagreement was found over the central/eastern US in June 2010 than in May, likely also due to the uncertainty in GEOS-Chem's soil or lightning NO_x emissions, which appear to be high over these regions (Figure S1). The NO_2 columns in the GEOS-Chem base simulation were overestimated in many northern China rural areas and underpredicted in a few urban areas in the East Asia as well as a broad area in the southwestern China. The mismatches between model and OMI NO_2 fell within the ranges of the comparison between the GOME2 NO_2 column product and six models' simulations over China in summer 2008 (Quennehen et al., 2016). Also, the use of monthly-mean anthropogenic emissions as well as the overall rough treatment of emission height and temporal profiles can be sources of uncertainty. These global model evaluation results suggest that the EAS-NAM SR relationships analyzed using this inventory may overall overestimate the NAM local contribution and underestimate the EAS contribution—Under different chemical regimes, this statement would also rely on the quality of other O_3 precursors' emissions in the HTAP2 inventory, and they may be associated with variable uncertainties depending on the species or emission sector as introduced in Section 2.1. Therefore, careful assessment of other key O_3 precursors' emissions in the inventory is needed in the future work. It is important to note that uncertainty in satellite retrievals can prevent us from producing accurate assessment on emissions (e.g., van Noije et al., 2006), and this comparison does not account for the biases in the used OMI data, and would be further validated by using other OMI NO_2 products as well as the bias-corrected (if applicable) in-situ NO_2 measurements. We also recommend more global models to save their calculations more frequently, at least near the satellite overpassing times, for a more comprehensive assessment of the emission inventory and a better understanding of the model biases.

3.1.2. Evaluation of the global model O_3 performance in NAM and EAS

The monthly-mean surface O_3 from multiple global models' free runs was evaluated with the CASTNET observations, at the stations with 95% of the hourly O_3 observation completeness for the 1 May-30 June 2010 period. The mean biases and RMSEs for these two months were summarized in Table 2a by US subregions. The three boundary condition-model as well as the eight-model ensembles overall underpredicted O_3 in the western US (by ~3-6 ppbv), similar to the HTAP1 model performance over these regions for May-June 2001 presented in Fiore et al. (2009). This can be due to the underestimated trans-boundary pollution (as indicated by the evaluation of modeled O_3 profiles with ozonesondes and satellite O_3 products). In addition, the coarser model resolutions are less capable of resolving the local features that influence the pollutants' import processes, chemical transformation, as well as regional processes such as the cross-state pollution transport over complex terrains. The global RAQMS base simulation with satellite assimilation improved the free tropospheric O_3 structure as its comparisons with the ozonesondes shows, which also enhanced the simulated monthly-mean surface O_3 by up to >10 ppbv in the western US and some coastal areas in the southeastern US (Figure S2, left). The global models overall significantly overestimated O_3 in the other three subregions (by 8-12 ppbv), close to HTAP1 model performance for May-June 2001 over the similar areas (Fiore et al., 2009) and in the Lapina et al. (2014) study for 2010, in large part due to the uncertainties in the bottom-up emissions as discussed in Section 3.1.1. Satellite assimilation led to 2-6 ppbv higher RAQMS surface O_3 in the central/southern/eastern US than in its free simulation, which are associated with higher positive biases.

The surface O_3 performance by individual global models varies significantly, e.g., with the RMSEs at all CASTNET sites ranging from ~9 ppbv to >15 ppbv (Table 2b). As reported in the literature (e.g., Geddes et al., 2016; Travis et al., 2016), the representation of land use/land cover, boundary layer mixing and chemistry can be sources of uncertainty for certain global model (i.e., GEOS-Chem), but how serious these issues were in the other models need to be investigated further. Some other possible reasons include the variation of these models' non-anthropogenic emission inputs and chemical mechanisms (Table 1c). Future work should emphasize on evaluating and comparing all models on process level to better understand their performance. Except in the northeastern US, the eight-model ensembles show better agreement with the CASTNET O_3 observations than the three boundary condition-model ensemble. Overall the three-model ensemble only outperforms one model but the eight-model ensemble outperforms seven individuals. This reflects that averaging the results from a larger number of models in this case more effectively cancelled out the positive or negative biases from the individual models.

The monthly-mean surface O_3 from multiple global models' free runs was also evaluated with the EANET observations. Among the three boundary condition models, GEOS-Chem produced higher O_3 than the other two throughout the year, and C-IFS O_3 is the lowest from April to December. The three-model and eight-model ensembles are lower than the surface O_3 observations by <10 ppbv during high O_3 seasons (winter/spring), but show substantial (>10 ppbv) positive biases during low O_3 seasons especially in July and August (Figure 3b), similar to the HTAP1 model performance over Japan in 2001 (Fiore et al., 2009). During May-June 2010, generally the models performed better at the Japanese sites than at the Korean sites (Table 2c), with significant positive biases occurring at low O_3 regions (e.g., in central Japan) and negative

biases found at high O_3 regions, mainly owing to the uncertainty in the local and upwind emissions. The different approaches to generate the monthly-mean modeled and the observed O_3 data may have also contributed to these model-observation discrepancies. Overall O_3 performance by individual models varies less significantly than at the CASTNET sites, with RMSEs ranging from 8.6 ppbv to ~13 ppbv (Table 2b). The three-model ensemble outperforms two individual models, and the eight-model ensemble outperforms six individual models. Unlike at the CASTNET sites, the three-model ensemble agrees better with the observations than the eight-model ensemble (Table 2c).

3.1.3. Evaluation of the STEM regional base simulations w/ three sets of boundary conditions

The three STEM base simulations using different boundary conditions were evaluated with the hourly O_3 observations at the CASTNET sites in the four US subregions. The evaluation included the 8 May-30 June 2010 period to exclude the results during the one-week spin-up period. The time series plots of observed and modeled O_3 at the western US CASTNET sites show that STEM was capable of capturing several high O_3 periods, and it produced larger biases during the nighttime (Figure 2c), as a result of the poorer WRF performance. Figure 2c and the evaluation statistics in Table 3a-b indicate that STEM/C-IFS O_3 concentrations are associated with the highest positive bias and RMSE, while the STEM/GEOS-Chem and STEM/RAQMS predictions were positively and negatively biased by less than 2 ppbv, respectively, with similar RMSEs and correlations with the observations. The quality of the three STEM simulation mean is closest to the STEM/GEOS-Chem run, with the mean bias/RMSE of ~1.6/4.9 ppbv, much better than the three-boundary model ensemble (-5.7/10.4 ppbv). However, this good performance can be a net effect of incorrect partitioning between the trans-boundary and local source contributions, with the former being underestimated and offsetting the overestimation of the latter. Switching the STEM chemical boundary conditions to the assimilated RAQMS base simulation led to increases in the simulated surface O_3 concentrations by >9 ppbv in the western US (Figure S2, right), associated with higher positive biases (due to several factors discussed in the next paragraph). Regional-scale assimilation could further reduce uncertainties introduced from regional meteorological and emission inputs to obtain better modeled total O_3 and the partitioning of trans-boundary versus US contributions (e.g., Huang et al., 2015).

The three STEM base simulations all significantly overpredicted O_3 over the rest of the US in part due to the overall overestimated NO_x emissions, with the STEM/RAQMS associated with the lowest RMSEs and mean biases, but STEM/C-IFS correlated best with the observations (Table 3b). These positive biases are higher than the global model ensembles', which can partially result from the possible unrealistic VOC speciation of the emission inventory and the SAPRC 99 chemical mechanism: Although SAPRC mechanisms have been used in air quality modeling for regulatory applications in some US states such as California, they usually produced higher O_3 than other mechanisms such as the CB04 and the CB05 (which were used by some HTAP2 global models, see Table 1c) over the US, and the comparisons between SAPRC 99 and SAPRC 2007 are still in progress (e.g., Luecken et al., 2008; Zhang et al., 2012; Cai et al., 2011). It is important to timely update the chemical mechanisms in the chemistry models, and we also suggest to timely upgrade the VOC speciation in the bottom-up emission inventories in the US to benefit the air quality modeling. Additionally, the uncertainty from non-anthropogenic emissions, such as the biogenic VOC emissions from WRF/MEGAN which is known to often have positive biases, can

be another cause: As Hogrefe et al. (2011) presented, the MEGAN emissions resulted in a higher O_3 response to hypothetical anthropogenic NO_x emission reductions compared with another set of biogenic emission input. Huang et al. (2017) showed that MEGAN's positive biases are in part due to the positively-biased temperature and radiation in WRF, and reducing ~2°C in WRF's temperature biases using a different land initialization approach led to ~20% decreases in MEGAN's isoprene emission estimates in September 2013 over some southeastern US regions. These temperature and radiation biases, can also be important sources of uncertainty in the modeled O_3 production. Quantifying the impacts of overestimated biogenic emissions and the biased weather fields that contributed to the biases in emissions on the modeled O_3 is still an ongoing work. Some existing studies also reported O_3 and NO_2 biases from other regional models in the eastern US, due to the chemical mechanism and biases in NO_x and biogenic VOC emissions (e.g., Canty et al., 2015). We anticipate that the results from the Air Quality Model Evaluation International Initiative (AQMEII) experiment (e.g., Schere et al., 2012; Solazzo et al., 2012; Galmarini et al., 2015, 2017), which involves more regional model simulations over the US with the similar set of boundary conditions but different chemical mechanisms and non-anthropogenic emission inputs, can help better understand the causes of errors in the simulated total O_3.

3.2. The NAM surface O_3 sensitivity to extra-regional anthropogenic pollutants

3.2.1. Global model ensembles

The impact of all foreign (i.e. non-NAM) anthropogenic sources on NAM surface O_3 was first explored, including the spatial distributions of the RERER metric (eq. (2)) based on various global models' simulations (Figure 5), and the domain wide mean sensitivities R (O_3, non-NAM, 20%) (eq. (1d)) (Figure 6). Across the NAM, the strongest impacts were found in spring time (March-April-May, larger than 1.5 ppbv in average over the domain) and the weakest impacts are shown during the summertime (June-July-August, 1.0-1.3 ppbv), consistent with the existing knowledge on the seasonal variability of the non-local pollution impacts on NAM for other years (e.g., Fiore et al., 2009; Reidmiller et al., 2009). All global models indicate strong non-NAM anthropogenic source impacts on the western US mainly due to the impact of its high elevation, and also near the US-Mexico border areas, especially southern Texas, due to their vicinity to the Mexican emission sources. Over the western states, stronger non-local impacts were reflected from the results based on higher-horizontal resolution global models (e.g., the >0.6 RERER values from the half degree EMEP model, corresponding to its higher R(O_3, non-NAM, 20%) values than the other models'), similar to the findings in previous modeling studies (Lin et al., 2010, 2012a). Although on a coarse horizontal resolution of 2.8°, OsloCTM3 suggests stronger extra-regional source influences on the northwestern US and the US-Canada border regions than the other models. Its largest number of vertical layers among all global models might be a cause. Larger-than-1 RERER values are often seen near the urban areas and large point sources due to the titration, especially evident from the higher resolution model results. The R(O_3, EAS, 20%) values are larger than 1/3 of the R(O_3, non-NAM, 20%) (0.2-0.5 ppbv from April to June), more than 3-4 times higher than R(O_3, EUR, 20%) and R(O_3, SAS, 20%). Note that all eight models contributed to the R(O_3, EAS, 20%) calculations, but one or two models did not provide all necessary sensitivity runs to compute the RERER, R(O_3, non-NAM, 20%), R(O_3, EUR, 20%), or R(O_3, SAS, 20%).

Comparing to the HTAP1 modeling results, the magnitudes of R(O_3, EUR, 20%) from this study are smaller by a factor of 2-3; In contrast, the R(O_3, non-NAM, 20%) and R(O_3, EAS, 20%)

values are >50% higher than the HTAP1 modeling results. The different HTAP1 and HTAP2 results are possibly due to the following three reasons: 1) the substantial improvement in the European air quality over the past decades that is shown in Crippa et al. (2016) and Pouliot et al. (2015), which contrasts with the growing anthropogenic emissions from the East Asia and other developing countries during 2001-2010; 2) the changes in the HTAP2 experiment setup from HTAP1. This includes the differences in the participating models, and the different region definitions, e.g., EUR by HTAP1's definition includes regions in Russia/Belarussia/Ukraine, Middle East and North Africa that are excluded from the HTAP2's EUR domain. For EAS and SAS, however, the regions not overlapped by HTAP1 and HTAP2 are mostly in the less populated/polluted regions; 3) the stronger-than-normal transport in 2010 than in 2000-2001, as first introduced in Section 2.2.1. Interannual variability of R(O_3, EAS, 20%) and R(O_3, non-NAM, 20%) is also found between 2010 and 2008-2009, based on the SNU GEOS-Chem calculations (Figure S3). Foreign anthropogenic pollution impact on NAM was stronger in 2010 than in 2008-2009, especially in April-May. This can be in part due to the higher O_3 precursors' emissions in 2010 from extra-regions including the East Asia (Table S1), as well as the spring 2010 meteorological conditions that favored the trans-Pacific pollution transport.

These monthly- and regional-mean R(O_3, EAS, 20%) values suggest that despite dilution along the great transport distance, the EAS anthropogenic sources still had distinguishable impact on the NAM surface O_3. Similar to the findings from the HTAP1 studies, the large intermodel variability (as indicated in Table 4) in the estimates of intercontinental SR relationships indicates the uncertainties of these models in representing the key atmospheric processes which needs more investigations in the future. Figure 6b compares the R(O_3, EAS, 20%) estimated by individual boundary condition models, their ensemble mean sensitivities, and the eight-global model mean. The averaged R(O_3, EAS, 20%) from the boundary condition model results are smaller than the eight-global model mean, and except for July-October 2010, GEOS-Chem gives higher R(O_3, EAS, 20%) than RAQMS and C-IFS, consistent with its highest O_3 prediction in the EAS source region (Figure 3b). Overall, R(O_3, EAS, 20%) and its intermodel differences are much smaller than the biases of the modeled total O_3 in NAM. Other factors can contribute more significantly to the biases in the modeled total O_3, such as the stratospheric O_3 intrusion and the local O_3 formation, and assessing the impacts from these factors would be also helpful for understanding the uncertainties in the modeled O_3.

The O_3 sensitivities in response to the perturbations of individual species or sector emissions in East Asia, estimated by the GEOS-Chem adjoint model, were also analyzed (Figure S3). These sensitivities show similar seasonal variability to R(O_3, EAS, 20%), with the values ~twice as high in the spring than in summer, also consistent with the results on previous years based on the 20% emission perturbation approach (e.g., Fiore et al., 2009; Brown-Steiner and Hess, 2011; Emmons et al., 2012). However, this seasonal variability is weaker than the results based on the tagged tracer approach for earlier years: Using the CAM-Chem model, Brown-Steiner and Hess (2011) reported that during the springtime, Asian O_3 created from the anthropogenic/biofuel NO_x emissions affected NAM O_3 ~three times as strongly as in summer. This is because the nonlinear O_3 chemistry, which is stronger outside of summer, caused larger O_3 responses to a 100% reduction of NO_x emissions than 5 times of the O_3 responses to a 20% reduction of NO_x emissions. The EAS anthropogenic NO_x emissions more strongly impacted the NAM surface O_3 than the other major O_3 precursors, similar to the findings in Fiore et al. (2009) and Reidmiller et al. (2009)

using the perturbation approach, as well as the conclusions in Lapina et al. (2014) based on the adjoint sensitivity analyses. Emissions from the power&industrial sectors are higher in East Asia than the other sectors (Table S1), resulting in its stronger influences on the NAM surface O_3. As the observed NO_2 columns started to drop since 2010 due to the effective denitration devices implemented at the Chinese power and industrial plants (e.g., Liu et al., 2016), depending on the changes in the VOC emissions, it is anticipated to see different R(O_3, EAS, 20%) values for the years after 2010. Therefore, continued studies to assess the East Asian anthropogenic pollution impacts on NAM during more recent years is needed. As emissions from various source sectors can differ by their emitted altitudes and temporal (from diurnal to seasonal) profiles, efforts should also be placed to have the models timely update the heights and temporal profiles of the emissions from those various sectors.

3.2.2. Regional model sensitivities and their connections with the boundary condition models'

The monthly-mean STEM surface R(O_3, EAS, 20%) sensitivities based on different boundary condition models were inter-compared, and also compared with the R(O_3, EAS, 20%) estimated by their boundary condition models as well as the global model ensemble mean (Figure 7). For both May and June 2010, the domain-wide mean R(O_3, EAS, 20%) values from STEM/RAQMS were higher than the estimates from RAQMS by 0.03 ppbv; the STEM/GEOS-Chem R(O_3, EAS, 20%) values are lower than those of GEOS-Chem by 0.01-0.06 ppbv, and the STEM/C-IFS R(O_3, EAS, 20%) is 0.02 ppbv higher than C-IFS's in June but slightly (<<0.01 ppbv) lower in May. These differences are overall smaller than the inter-global model differences, and can be due to various factors including the uncertainties in boundary condition chemical species mapping, and the different meteorological/terrain fields/chemistry in the global and regional model pairs. The STEM R(O_3, EAS, 20%) ensemble mean values, however, are less than 0.02 ppbv different from its boundary condition model's ensemble mean for both months. The STEM R(O_3, EAS, 20%) ensemble mean value in June is also close to the eight-global model ensemble mean, but is ~0.05 ppbv lower than the eight-model mean in May. Choosing other/more global model outputs as STEM's boundary conditions may lead to different STEM ensemble mean R(O_3, EAS, 20%) estimates. We also found that the period mean R(O_3, EAS, 20%) of ~0.2 ppbv sampled only at the CASTNET sites (Table 3a) are smaller than those averaged in all model grids. This indicates that currently the sparsely distributed surface network (especially over the western US that is more strongly affected by the extra-regional sources than the other US regions) may miss many LRT episodes that impact the NAM. The planned geostationary satellites with ~2-5 km footprint sizes and hourly sampling frequency (Hilsenrath and Chance, 2013) will help better capture the high O_3 and LRT episodes in these regions.

The spatial patterns of the monthly-mean STEM surface R(O_3, EAS, 20%) sensitivities based on the three boundary condition models are notably different, but overall resemble what's estimated by the corresponding boundary condition model, and the STEM sensitivities show more local details in certain high elevation regions in the US west (Figure 8 shows the June 2010 conditions as an example). These different sensitivities were investigated further, by examining the R(O_3, EAS, 20%) values near the source regions (i.e., East Asia) as well as near the receptor regions (Figure 9). More East Asian anthropogenic O_3 seems to be transported at the upper troposphere in RAQMS than in the other two models. GEOS-Chem and RAQMS R(O_3, EAS, 20%) sensitivities are similar over the EAS as well as the 500-900 hPa near the receptor in the eastern

Pacific (at ~135°W), the altitudes US surface O_3 are most strongly sensitive to during the summertime as concluded from previous studies (e.g., Huang et al., 2010, 2013a; Parrish et al., 2010). Despite the close NAM domain-wide mean values from the STEM/GEOS-Chem and STEM/RAQMS, the spatial patterns of R(O_3, EAS, 20%) over NAM differ in these two cases, with the latter case showing sharper gradients especially in the western US, partially due to the impact of its higher horizontal resolution. The R(O_3, EAS, 20%) values from STEM/C-IFS are lower than from the other two cases both near the sources and at (near) NAM. The STEM surface (also near surface, not shown in figures) R(O_3, EAS, 20%) does not spatially correlate well with the column R(O_3, EAS, 20%), the latter of which contributed more to the base case O_3 columns, indicating that a good portion of the transported East Asian pollution did not descend to the lower altitudes to impact the boundary layer/ground level air quality. An additional regional simulation was performed in which the STEM boundary conditions were downscaled from a RAQMS simulation without the East Asian anthropogenic emissions. The non-linear emission perturbation-O_3 response relationships, as the larger-than-1 S_{o3} metric (eq. (3)) indicate, are seen across the domain, for both the surface and column O_3 (Figure 8). S_{o3} for column O_3, ranging from 1.15-1.25 in most regions, are overall ~0.05 higher than S_{o3} for the surface O_3. Therefore, the full source contribution obtained by linearly scaling the receptor regional mean O_3 sensitivity to the 20% reduction in the source region emissions may be underestimated by at least ~10%.

3.2.3. Regional model MDA8 sensitivities on all days and during the O_3 exceedances

The temporal variability of the STEM R(O_3, EAS, 20%) ensemble sensitivities were also studied. For most US subregions, 3-6 LRT episodes (defined as when the sensitivities are above the period mean) were identified during May-June. Throughout this period, the hourly R(O_3, EAS, 20%) and the observed O_3 at the surface CASTNET sites are weakly correlated (Table 3a), but they display similar diurnal cycles (e.g., Figures 2c and 2d for the western US sites), possibly because the deeper boundary layer depth during the daytime enhanced entrainment down-mixing of the extra-regional pollutants to the surface. The identified diurnal variability of the R(O_3, EAS, 20%) can cause differences in the calculated MDA8 and all-hour mean R(O_3, EAS, 20%) values. Figure S4 shows that the mean R(MDA8, EAS, 20%) values, usually at daytimes, are higher than the all-hour averaged R(O_3, EAS, 20%) in most STEM model grids during both months. Therefore, it is important for more HTAP2 participating models to save their outputs hourly in order to conveniently compute the policy-relevant metrics for the O_3 sensitivities. Also, the hourly sampling frequency of the planned geostationary satellites is anticipated to be more helpful for evaluating the impacts of the LRT episodes.

The STEM R(MDA8, EAS, 20%) in all model grids within the four US subregions were averaged on all days during May-June 2010 and only on the days when the simulated total MDA8 O_3 is over 70 ppbv (Figure 10). These sensitivities also show appreciable spatial variability: from 0.35-0.58 ppbv in the western US (also with the largest standard deviations, not shown), which is slightly higher than the HTAP1 results reported by Reidmiller et al. (2009) for Spring 2001, to ~0.1-0.25 ppbv in the rest three subregions, which is close to the Reidmiller et al. (2009) results.

Comparing the solid bar plots in Figures 10-11, we found that on all days in the three non-western subregions, R(MDA8, EAS, 20%) values sampled at CASTNET sites are slightly smaller than those computed for all model grids, while in the non-western states the opposite differences

are seen. This again suggests that expanding observation network would help better capture the high O_3 and LRT episodes.

Figure 10 suggests smaller R(MDA8, EAS, 20%) values during the high O_3 days in all subregions. However, STEM's total O_3 concentrations at CASTNET sites during the O_3 exceedances were substantially overpredicted in non-western US regions while significantly underpredicted in the western US (see mean biases above the bar plots in Figure 11). Therefore, the R(MDA8, EAS, 20%) values shown in Figure 10 during O_3 exceedances can actually represent the sensitivities during the non-exceedances in non-western US regions, and may not represent the sensitivities during all O_3 exceedances in the western US. Figures 11-12 show that if calculated only at the CASTNET sites during the exceedances, in non-western US regions, R(MDA8, EAS, 20%) is 0.02-0.07 ppbv smaller during the high O_3 total days. This is qualitatively consistent with the findings in Reidmiller et al. (2009), and is possibly because that the LRT impacts were stronger on some days with good dispersion conditions when the NAAQS was not exceeded, but weaker on some high O_3 days under stagnant conditions. In contrast, western US R(MDA8, EAS, 20%) at CASTNET sites was ~0.05 ppbv higher on high O_3 days than for all days, and this differences are larger in rural/remote areas where local influences are less dominant. As a result, the medium/strong positive correlations are found between modeled LRT of pollution and the total O_3 in these regions (Table 3a; Lin et al., 2012a).

3.3. Case studies of spring (9 May) and summer (10 June) LRT events mixed with stratospheric O_3 intrusions

Lin et al. (2012a, b) and Neuman et al. (2012) showed that the trans-Pacific pollution transport intensely impacted the western US during 8-10 May, 2010, intermingled with a stratospheric intrusion that contributed to at least 1/3 of the total O_3 in some high elevation regions. This episode is indeed indicated by the O_3 and CO products from AIRS and TES at ~500 hPa over the Eastern Pacific (Figure 13), and the observed TES and IASI O_3 profiles over the western US indicated elevated O_3 levels (>80 ppbv) at 700-900 hPa. Huang et al. (2013b) found that the meteorological conditions during this period (i.e., a strong jet at ~700 hPa with wind speed >20 m/s shifted southwesterly when passing the southern California and continued to travel towards the mountain states), along with the orographic lifting, efficiently exported the southern California anthropogenic pollution, which was chemically coupled with the extra-regional pollution and significantly enhanced the O_3 levels in the US intermountain west.

We selected this episode to compare the STEM surface total O_3 concentrations as well as the R(O_3, EAS, 20%) sensitivities based on the different HTAP2 boundary condition models. Figure 14 evaluates the simulated O_3 profiles in the western US from several STEM base simulations against the TES and IASI O_3 retrievals, and Figures 15a-d indicate the performance of the daily surface total MDA8 O_3 from these simulations. We found that the underestimated free tropospheric O_3 from the STEM simulations that used any single free-running chemical boundary conditions contributed to the underestimated STEM surface O_3 in the high elevation mountain states: e.g., by 9-14 ppbv at three CASTNET sites (Grand Canyon National Park (NP), AZ; Canyonlands NP, UT; and Rocky Mountain NP, CO) where O_3 exceedances were observed. The unsatisfactory performance by free-running global models during high O_3 events would pose difficulties for regional models (regardless of their resolutions and other configurations,

parameterization) to accurately estimate the SR relationships using boundary conditions downscaled from these model runs. The STEM base simulation using the RAQMS assimilated fields as the boundary conditions, agrees most with the observed O_3 at the CASTNET sites, as well as the TES and IASI O_3 profiles in the western states. Similar to the conclusions drawn in Huang et al. (2010, 2015) for summer 2008, we again demonstrated the robustness of satellite chemical data assimilation for improving the boundary condition models' O_3 performance. As the enhancement of O_3 due to the assimilation is much larger than the O_3 sensitivities to the EAS anthropogenic emissions, the assimilation mainly improved the contributions from other sources, such as the stratospheric O_3.

The quality of the model boundary conditions only indicates how well the total "transported background" component is represented, and can not be directly connected with the accuracy of the model estimated R(O_3, EAS, 20%) sensitivities, which also show notable intermodel differences: The estimated R(MDA8, EAS, 20%) in the different STEM cases range from <1.0 ppbv to ~1.3 ppbv, at least 40% higher than the May-June period mean in Figures 10-11. The mean R(MDA8, EAS, 20%) at three high O_3 CASTNET sites range from 0.73 (STEM/GEOS-Chem) to 0.98 ppbv (STEM/C-IFS), with the mean S_{O3} of ~1.14 at these sites based on the STEM/RAQMS runs due to the nonlinear emission perturbation-O_3 response relationships (Figure 15e-h). The R(MDA8, EAS, 100%) from the STEM/RAQMS case is as high as >7 ppbv over the high terrain regions. These are of smaller magnitudes than the estimates in Lin et al. (2012a), possibly due to the differences in the used models and the bottom-up emission inputs.

A stratospheric O_3 intrusion also affected the NE US on the same day, as revealed by the satellite free tropospheric O_3 and CO observations (Figure 13). This intrusion was mixed with LRT East Asian pollution (Figure 15 and Figure S5). However, this intrusion did not enhance the NE boundary layer/surface O_3 concentrations, which were actually anomalously low (MDA8<40 ppbv) as indicated by the model base simulations and the CASTNET observations (Figure 15a-d). Similar characteristics during summertime stratospheric O_3 intrusion events around this region have been discussed by Ott et al. (2016). The East Asian pollution less intensely (<50%) affected the surface O_3 levels in these regions than in the US west, due to the greater transport distances, stronger local emission influence on chemical production/loss, as well as the impact of the overall flat terrain in the US east.

A summertime LRT event on 9-10 June is analyzed to contrast with the 9 May case study. Lin et al. (2012b) showed that >80 ppbv of ozonesonde data in northern California at 2-6 km measured the stratospheric O_3 remnants during this episode, and the transported stratospheric O_3 contributed to as much as ~50% of the total O_3 in southern California based on their model calculations. We show that on 10 June over 100 ppbv of O_3, as well as <90 ppbv CO, was observed by satellites at ~500 hPa above Nevada and northern California (Figure 16), which again was substantially underestimated by all free-running models (Figure 17), resulting in the underpredicted total O_3 at two CASTNET sites in southern California (Converse Station and Joshua Tree NP) that experienced O_3 exceedances on this day (Figure 18a-c). The negative biases in the "transported background" O_3 and surface MDA8 O_3 were successfully reduced by incorporating satellite data (Figures 17 and 18d).

Figures 18e-h show that LRT of EAS anthropogenic pollution also strongly affected southern California and Nevada. Notable intermodel differences are again found in the estimated R(MDA8, EAS, 20%), but they are overall lower than on 9 May (<1.0 ppbv). The mean R(MDA8, EAS, 20%) at the two high O_3 CASTNET sites range from 0.54 (STEM/C-IFS) to 0.86 ppbv (STEM/RAQMS), with the mean S_{O3} of ~1.13 at these sites based on the STEM/RAQMS runs (Figure 18e-h). The R(MDA8, EAS, 100%) from the STEM/RAQMS case is as high as >6 ppbv over southern California and Nevada. Compared to the spring event, R(MDA8, EAS, 20%) in the eastern US are discernable only over a limited region, due to weaker transport and stronger local chemical production/loss.

4. Conclusions and suggestions on future directions

In support of the HTAP Phase 2 experiment that involved high-resolution global models and regional models' participation to advance the understanding of the pollutants' SR relationships in the Northern Hemisphere, we conducted a number of regional scale STEM base and forward sensitivity simulations over NAM during May-June 2010. STEM's top and lateral chemical boundary conditions were downscaled from three global models' (i.e., GEOS-Chem, RAQMS, and ECMWF C-IFS) base and sensitivity simulations (in which the East Asian anthropogenic emissions were reduced by 20%). Despite dilution along the great transport distance, the East Asian anthropogenic sources still had distinguishable impact on the NAM surface O_3, with the period-mean NAM O_3 sensitivities to a 20% reduction of the East Asian anthropogenic emissions (i.e., R(O_3, EAS, 20%)) ranging from ~0.24 ppbv (STEM/C-IFS) to ~0.34 ppbv (STEM/RAQMS). The spatial patterns of the STEM surface O_3 sensitivities over NAM overall resembled those from its corresponding boundary condition model, with regional/period mean R(O_3, EAS, 20%) differed slightly (<10%) from its corresponding boundary condition model's, which are smaller than those among its boundary condition models. The boundary condition models' two-month mean R(O_3, EAS, 20%) was ~8% lower than the mean sensitivity estimated by multiple global models. Therefore, choosing other global model outputs as STEM's boundary conditions may lead to different STEM O_3 sensitivities. The biases and RMSEs in the simulated total O_3, which differed significantly among models, can partially be due to the uncertainty in the bottom-up NO_x emission inputs according to the model comparison with the OMI NO_2 columns, and future work on attributing the intermodel differences on process level is particularly important for better understanding the sources of uncertainties in the modeled total O_3 and its source contribution.

The HTAP2 multi-model ensemble mean R(O_3, EAS, 20%) values in 2010 were higher than the HTAP1 reported 2001 conditions, due to the impacts of the growing East Asian anthropogenic emissions, the interannual variability in atmospheric circulation (i.e., stronger trans-Pacific transport in spring 2010 following an El Niño event), and the different experiment designs of HTAP1 and HTAP2. The GEOS-Chem O_3 sensitivities in 2010 were also higher than the 2008-2009 conditions due to the increasing Asian emissions and the spring 2010 meteorological conditions that favored the trans-Pacific pollution transport. The GEOS-Chem sensitivity calculations indicate that the East Asian anthropogenic NO_x emissions mattered more than the other East Asian O_3 precursors to the NAM O_3, qualitatively consistent with previous adjoint sensitivity calculations. Continued research is needed on temporal changes of emissions for different species and sectors in NAM and foreign countries as well as their impacts on the SR relationships. As emissions from various source sectors can differ by emitted altitudes and

temporal profiles, efforts should also be placed to have the models timely update the height and temporal profiles of the emissions from various sectors.

An additional STEM simulation was performed in which the boundary conditions were downscaled from a RAQMS simulation without East Asian anthropogenic emissions (i.e., a 100% emission reduction), to assess the scalability of the mean O_3 sensitivities to the size of the emission perturbation. The scalability was found to be spatially varying, ranging from 1.15-1.25 for column O_3 in most US regions, which were overall ~0.05 higher than the surface O_3's. Therefore, the full source contribution obtained by linearly scaling the NAM regional mean O_3 sensitivity to the 20% reduction in the East Asian emissions may be underestimated by at least 10%. The underestimation in other seasons of the HTAP2 study period may be higher and will need to be quantified in future work. Also, motivated by Lapina et al. (2014), additional calculations will be conducted in future to explore the scalability of different O_3 metrics in these cases. For future source attribution analysis, in general it is recommended to directly choose the suitable size of the emission perturbation based on the specific questions to address, and to avoid linearly scaling O_3 sensitivities that are based on other amounts of the perturbations.

The STEM O_3 sensitivities to the East Asian anthropogenic emissions (based on three boundary condition models separately and averagely) were strong during 3-6 episodes in May-June 2010, following similar diurnal cycles as the total O_3. Stronger-than-normal East Asian anthropogenic pollution impacts were estimated during O_3 exceedances in the western US, especially over the high terrain rural/remote areas; in contrast, non-local pollution impacts were less strong during O_3 exceedances in other US regions. We emphasized the importance of saving model results hourly for continently calculate policy-relevant metrics, as well as the usefulness of hourly sampling frequency of the planned geostationary satellites for better evaluating the impacts of the LRT events.

Based on model calculations, satellite O_3 (TES, JPL-IASI, and AIRS), CO (TES and AIRS) and surface O_3 observations on 9 May 2010, we showed the different influences from stratospheric O_3 intrusions along with the transported East Asian pollution on O_3 in the western and the eastern US. This event was further compared with a summer event of 10 June 2010. During both events, the unsatisfactory performance of free-running global models would pose difficulties for regional models (regardless of their resolutions and other configurations, parameterization) to accurately simulate the surface O_3 and its source contribution using boundary conditions downscaled from these model runs. Incorporating satellite (OMI and MLS) O_3 data effectively improved the modeled O_3. As chemical data assimilation techniques keep developing (Bocquet et al., 2015), several HTAP2 participating global models have already been able to assimilate single- or multi-constitute satellite atmospheric composition data (e.g., Miyazaki et al., 2012; Parrington et al., 2008, 2009; Huang et al., 2015; Inness et al., 2015; Flemming et al., 2017). Comparing the performance of the assimilated fields from different models, and making the global model assimilated chemical fields in the suitable format for being used as boundary conditions would be very beneficial for future regional modeling, as well as for better interpreting the pollutants' distributions especially during the exceptional events. Meanwhile, efforts should also be devoted to advancing and applying higher-resolution regional scale modeling and chemical data assimilation. Furthermore, although satellite observations have been applied for improving the estimated US background O_3 (e.g., Huang et al., 2015), using satellite (and/or other types of)

observations to improve SR relationship studies also needs to be explored. Some of the possible methods include: 1) The combination of data assimilation and the tagging approach; 2) Introducing observation-constrained emission estimates in the emission perturbation analyses.

Acknowledgements

The global and regional modeling results used in this study have been submitted to the AeroCom database following the HTAP2 data submission guidelines (http://iek8wikis.iek.fz-juelich.de/HTAPWiki/HTAP-2-data-submission), or can be made available upon request. Technical support from Anna Carlin Benedictow, Brigitte Koffi, Jan Griesfeller, and Michael Schulz regarding formatting and submitting the data to the AeroCom is acknowledged. MH thanks the research resources at the University of Iowa and JPL/Caltech that supported this study, as well as the travel funding from the US EPA for attending the related HTAP2 workshops. DKH and YD recognize support from NASA AQAST. FD Acknowledges support from the Administrative Arrangement. Part of this research was carried out at the Jet Propulsion Laboratory, California Institute of Technology, under contract to the National Aeronautics and Space Administration. Reference herein to any specific commercial product, process or service by trade name, trademark, manufacturer or otherwise does not constitute or imply its endorsement by the United States Government or the Jet Propulsion Laboratory, California Institute of Technology. The views, opinions, and findings contained in this report are those of the author(s) and should not be construed as an official National Oceanic and Atmospheric Administration or U.S. Government position, policy, or decision. We also acknowledge the feedbacks from Dr. Gail Tonnesen, two anonymous reviewers, and Dr. Meiyun Lin on earlier versions of this paper, that helped improve its quality.

References

Anderson, D. C., Loughner, C. P., Diskin, G., Weinheimer, A., Canty, T., P., Salawitch, R. J., Worden, H. M., Fried, A., 25 Mikoviny, T., Wisthaler, A., and Dickerson, R., R. (2014), Measured and modeled CO and NO_y in DISCOVER-AQ: An evaluation of emissions and chemistry over the eastern US, Atmos. Environ., 96, 78-87, doi: 10.1016/j.atmosenv.2014.07.004.

Allen, D. J., Pickering, K. E., Pinder, R. W., Henderson, B. H., Appel, K. W., and Prados, A. (2012), Impact of lightning-NO on eastern United States photochemistry during the summer of 2006 as determined using the CMAQ model, Atmos. Chem. Phys., 12, 1737-1758, doi: 10.5194/acp-12-1737-2012.

Ambrose, J.L., Reidmiller, D.R., and Jaffe, D.A. (2011), Causes of high O_3 in the lower free troposphere over the Pacific Northwest as observed at the Mt. Bachelor Observatory. Atmos. Environ., 45, 5302–5315, doi: 10.1016/j.atmosenv.2011.06.056.

Anenberg, S. C., L. W. Horowitz, D. Q. Tong, and J. J. West (2010), An estimate of the global burden of anthropogenic ozone and fine particulate matter on premature human mortality using atmospheric modeling, Environ. Health Perspect., 118(9), 1189–1195.

Avnery, S, D.L. Mauzerall, J. Liu, L.W. Horowitz (2011a), Global Crop Yield Reductions due to Surface Ozone Exposure: 1. Year 2000 Crop Production Losses and Economic Damage, Atmos. Environ., 45, 2284-2296.

Avnery, S, D.L. Mauzerall, J. Liu, L.W. Horowitz (2011b), Global Crop Yield Reductions due to Surface Ozone Exposure: 2. Year 2030 Potential Crop Production Losses and Economic Damage under Two Scenarios of O_3 Pollution, Atmos. Environ., 45, 2297-2309.

Beer, R., T. A. Glavich, and D. M. Rider (2001), Tropospheric emission spectrometer for the Earth Observing System's Aura satellite, Applied Optics, 40, 2356 – 2367.

Beer, R (2006), TES on the Aura Mission: Scientific Objectives, Measurements, and Analysis Overview, IEEE Transaction on Geoscience and Remote Sensing, 44, 1102-1105.

Bian, J., A. Gettelman, H. Chen, and L. L. Pan (2007), Validation of satellite ozone profile retrievals using Beijing ozonesonde data, J. Geophys. Res., 112, D06305, doi:10.1029/2006JD007502.

Bocquet, M., Elbern, H., Eskes, H., Hirtl, M., Žabkar, R., Carmichael, G. R., Flemming, J., Inness, A., Pagowski, M., Pérez Camaño, J. L., Saide, P. E., San Jose, R., Sofiev, M., Vira, J., Baklanov, A., Carnevale, C., Grell, G., and Seigneur, C. (2015), Data assimilation in atmospheric chemistry models: current status and future prospects for coupled chemistry meteorology models, Atmos. Chem. Phys., 15, 5325-5358, doi:10.5194/acp-15-5325-2015.

Boersma, K. F., Braak, R., van der A, R. J. (2011a), Dutch OMI NO_2 (DOMINO) data product v2.0 HE5 data file user manual. http://www.temis.nl/docs/OMI_NO2_HE5_2.0_2011.pdf.

Boersma, K. F., Eskes, H. J., Dirksen, R. J., van der A, R. J., Veefkind, J. P., Stammes, P., Huijnen, V., Kleipool, Q. L., Sneep, M., Claas, J., Leitão, J., Richter, A., Zhou, Y., Brunner, D. (2011b), An improved tropospheric NO_2 column retrieval algorithm for the Ozone Monitoring Instrument, Atmos. Meas. Tech., 4, 1905-1928.

Bowman, K. W., Rodgers, C. D., Kulawik, S. S., Worden, J., Sarkissian, E., Osterman, G., Steck, T., Lou, M., Eldering, A., Shephard, M., Worden, H., Lampel, M., Clough, S., Brown, P., Rinsland, C., Gunson, M., and Beer, R. (2006), Tropospheric Emission Spectrometer: Retrieval method and error analysis, IEEE Transaction on Geoscience and Remote Sensing, 44 (5), 1297–1307, doi: 10.1109/TGRS.2006.871234.

Bowman, K., and D. K. Henze (2012), Attribution of direct ozone radiative forcing to spatially resolved emissions, Geophys. Res. Lett., 39, L22704, doi:10.1029/2012GL053274.

Brioude, J., Angevine, W. M., Ahmadov, R., Kim, S.-W., Evan, S., McKeen, S. A., Hsie, E.-Y., Frost, G. J., Neuman, J. A., Pollack, I. B., Peischl, J., Ryerson, T. B., Holloway, J., Brown, S. S., Nowak, J. B., Roberts, J. M., Wofsy, S. C., Santoni, G. W., Oda, T., and Trainer, M. (2013), Top-down estimate of surface flux in the Los Angeles Basin using a mesoscale inverse modeling technique: assessing anthropogenic emissions of CO, NO_x and CO_2 and their impacts, Atmos. Chem. Phys., 13, 3661-3677, doi:10.5194/acp-13-3661-2013.

Brown-Steiner, B., and P. Hess (2011), Asian influence on surface ozone in the United States: A comparison of chemistry, seasonality, and transport mechanisms, J. Geophys. Res., 116, D17309, doi:10.1029/2011JD015846.

Cai, C., J. T. Kelly, J. C. Avise, A. P. Kaduwela, and W. R. Stockwell (2011), Photochemical Modeling in California with Two Chemical Mechanisms: Model Intercomparison and Response to Emission Reductions, J. Air & Waste Manage. Assoc., 61:5, 559-572, doi: 10.3155/1047-3289.61.5.559.

Canty, T. P., Hembeck, L., Vinciguerra, T. P., Anderson, D. C., Goldberg, D. L., Carpenter, S. F., Allen, D. J., Loughner, C. P., Salawitch, R. J., and Dickerson, R. R. (2015), Ozone and NOx chemistry in the eastern US: evaluation of CMAQ/CB05 with satellite (OMI) data, Atmos. Chem. Phys., 15, 10965-10982, doi:10.5194/acp-15-10965-2015.

Carmichael, G.R., Tang, Y., Kurata, G., Uno, I., Streets, D.G., Thongboonchoo, N., Woo, J.H., Guttikunda, S., White, A., Wang, T., Blake, D.R., Atlas, E., Fried, A., Potter, B., Avery, M.A., Sachse, G.W., Sandholm, S.T., Kondo, Y., Talbot, R.W., Bandy, A., Thorton, D., and Clarke, A.D. (2003a), Evaluating regional emission estimates using the TRACE-P observations, J. Geophys. Res., 108 (D21), 8810, doi: 10.1029/2002JD003116.

Carmichael, G.R., Tang, Y., Kurata, G., Uno, I., Streets, D., Woo, J.H., Huang, H., Yienger, J., Lefer, B., Shetter, R., Blake, D., Atlas, E., Fried, A., Apel, E., Eisele, F., Cantrell, C., Avery, M., Barrick, J., Sachse, G., Brune, W., Sandholm, S., Kondo, Y., Singh, H., Talbot, R., Bandy, A., Thorton, D., Clarke, A., and Heikes, B. (2003b), Regional-scale chemical transport modeling in support of the analysis of observations obtained during the TRACE-P experiment, J. Geophys. Res., 108 (D21), 8823, doi: 10.1029/2002JD003117.

Carter, W. P. L. (2000), Documentation of the SAPRC-99 chemical mechanism for VOC Reactivity Assessment, final report to California Air Resources Board, Contract No. 92-329 and 95-308.

Cooper, O. R., et al. (2010), Increasing springtime ozone mixing ratios in the free troposphere over western North America, Nature, 463, doi: 10.1038/nature08708.

Cooper, O. R., Oltmans, S. J., Johnson, B. J., Brioude, J., Angevine, W., Trainer, M., Parrish, D. D., Ryerson, T. R., Pollack, I., Cullis, P. D., Ives, M. A., Tarasick, D. W., Al-Saadi, J., and Stajner, I. (2011), Measurement of western U.S. baseline ozone from the surface to the tropopause and assessment of downwind impact regions, J. Geophys. Res., 116, D00V03, doi: 10.1029/2011JD016095.

Cooper, O., et al. (2016), Western NA Performance Evaluation for HTAP2, HTAP2 workshop, Potsdam, Germany, 2016.

Crippa, M., Janssens-Maenhout, G., Dentener, F., Guizzardi, D., Sindelarova, K., Muntean, M., Van Dingenen, R., and Granier, C. (2016), Forty years of improvements in European air quality: regional policy-industry interactions with global impacts, Atmos. Chem. Phys., 16, 3825-3841, doi:10.5194/acp-16-3825-2016.

Emmons, L. K., Hess, P. G., Lamarque, J.-F., and Pfister, G. G. (2012), Tagged ozone mechanism for MOZART-4, CAM-chem and other chemical transport models, Geosci. Model Dev., 5, 1531-1542, doi:10.5194/gmd-5-1531-2012.

Eskes, H. J. and Boersma, K. F. (2003), Averaging kernels for DOAS total-column satellite retrievals, Atmos. Chem. Phys., 3, 1285-1291.

Fiore, A. M., et al. (2009), Multimodel estimates of intercontinental source receptor relationships for ozone pollution, J. Geophys. Res., 114, D04301, doi:10.1029/2008JD010816.

Fiore, A. M., J. T. Oberman, M. Y. Lin, L. Zhang, O. E. Clifton, D. J. Jacob, V. Naik, L. W. Horowitz, J. P. Pinto, and G. P. Milly (2014), Estimating North American background ozone in U.S. surface air with two independent global models: Variability, uncertainties, and recommendations, Atmos. Environ., 96, 284–300, doi: 10.1016/j.atmosenv.2014.07.045.

Flemming, J., Huijnen, V., Arteta, J., Bechtold, P., Beljaars, A., Blechschmidt, A.-M., Diamantakis, M., Engelen, R. J., Gaudel, A., Inness, A., Jones, L., Josse, B., Katragkou, E., Marecal, V., Peuch, V.-H., Richter, A., Schultz, M. G., Stein, O., and Tsikerdekis, A. (2015), Tropospheric chemistry in the Integrated Forecasting System of ECMWF, Geosci. Model Dev., 8, 975-1003, doi:10.5194/gmd-8-975-2015.

Flemming, J., Benedetti, A., Inness, A., Engelen, R., Jones, L., Huijnen, V., Remy, S., Parrington, M., Suttie, M., Bozzo, A., Peuch, V.-H., Akritidis, D., and Katragkou, E. (2017), The CAMS

interim Reanalysis of Carbon Monoxide, Ozone and Aerosol for 2003–2015, Atmos. Chem. Phys., 17, 1945-1983, doi:10.5194/acp-17-1945-2017.
Galmarini, S., C. Hogrefe, D. Brunner, P. Makar, A. Baklanov (2015), Preface to the AQMEII p2 Special issue, Atmos. Environ., 115, 340-344.
Galmarini, S., Koffi, B., Solazzo, E., Keating, T., Hogrefe, C., Schulz, M., Benedictow, A., Griesfeller, J. J., Janssens-Maenhout, G., Carmichael, G., Fu, J., and Dentener, F. (2017), Technical note: Coordination and harmonization of the multi-scale, multi-model activities HTAP2, AQMEII3, and MICS-Asia3: simulations, emission inventories, boundary conditions, and model output formats, Atmos. Chem. Phys., 17, 1543-1555, doi:10.5194/acp-17-1543-2017.
Geddes, J. A., Heald, C. L., Silva, S. J., and Martin, R. V. (2016), Land cover change impacts on atmospheric chemistry: simulating projected large-scale tree mortality in the United States, Atmos. Chem. Phys., 16, 2323-2340, doi:10.5194/acp-16-2323-2016.
Gery, M. W., G. Z. Whitten, J. P. Killus, and M. C. Dodge (1989), A photochemical kinetics mechanism for urban and regional scale computer modeling, J. Geophys. Res., 94, 12,925 – 12,956, doi:10.1029/JD094iD10p12925.
Granier, C., Lamarque, J. F., Mieville, A., Muller, J. F., Olivier, J., Orlando, J., Peters, J., Petron, G., Tyndall, G., and Wallens, S. (2005), POET, a database of surface emissions of ozone precursors, http://www.aero.jussieu.fr/projet/ACCENT/POET.php.
Gratz, L.E., Jaffe, D.A., and Hee, J.R. (2014), Causes of increasing ozone and decreasing carbon monoxide in springtime at the Mt. Bachelor Observatory from 2004 to 2013, Atmos. Environ., 109, 323–330, doi: 10.1016/j.atmosenv.2014.05.076.
Guenther, A. B., X. Jiang, C. L. Heald, T. Sakulyanontvittaya, T. Duhl, L. K. Emmons, and X. Wang (2012), The Model of Emissions of Gases and Aerosols from Nature version 2.1 (MEGAN2.1): an extended and updated framework for modeling biogenic emissions, Geosci. Model Dev., 5 (6), 1471-1492.
Henze, D. K., Hakami, A., and Seinfeld, J. H. (2007), Development of the adjoint of GEOS-Chem, Atmos. Chem. Phys., 7, 2413–2433, doi:10.5194/acp-7-2413-2007.
Hilsenrath, E., and K. Chance (2013), NASA ups the TEMPO on monitoring air pollution, Earth Obs., 25, 10–15.
Hogrefe, C., Isukapalli, S., Tang, X., Georgopoulos, P., He, S., Zalewsky, E., Hao, W., Ku, J., Key, T., and Sistla, G. (2011), Impact of biogenic emission uncertainties on the simulated response of ozone and fine Particulate Matter to anthropogenic emission reductions, J. Air Waste Manage., 61, 92–108.
Huang, M., Carmichael, G. R., Adhikary, B., Spak, S. N., Kulkarni, S., Cheng, Y. F., Wei, C., Tang, Y., Parrish, D. D., Oltmans, S. J., D'Allura, A., Kaduwela, A., Cai, C., Weinheimer, A. J., Wong, M., Pierce, R. B., Al-Saadi, J. A., Streets, D. G., and Zhang, Q. (2010), Impacts of transported background ozone on California air quality during the ARCTAS-CARB period – a multi-scale modeling study, Atmos. Chem. Phys., 10, 6947-6968, doi: 10.5194/acp-10-6947-2010.
Huang, M., Carmichael, G. R., Chai, T., Pierce, R. B., Oltmans, S. J., Jaffe, D. A., Bowman, K. W., Kaduwela, A., Cai, C., Spak, S. N., Weinheimer, A. J., Huey, L. G., and Diskin, G. S. (2013a), Impacts of transported background pollutants on summertime western US air quality: model evaluation, sensitivity analysis and data assimilation, Atmos. Chem. Phys., 13, 359-391, doi: 10.5194/acp-13-359-2013.

1117 Huang, M., Bowman, K. W., Carmichael, G. R., Pierce, R. B., Worden, H. M., Luo, M., Cooper,
1118 O. R., Pollack, I. B., Ryerson, T. B., Brown, S. S. (2013b), Impact of southern California
1119 anthropogenic emissions on ozone pollution in the mountain states, J. Geophys. Res., 118,
1120 12784-12803, doi: 10.1002/2013JD020205.
1121 Huang, M., et al. (2014), Changes in nitrogen oxides emissions in California during 2005–2010
1122 indicated from top-down and bottom-up emission estimates, J. Geophys. Res., 119, 12,928–
1123 12,952, doi: 10.1002/2014JD022268, 2014.
1124 Huang, M., et al. (2015), Improved Western US Background Ozone Estimates via Constraining
1125 Nonlocal and Local Source Contributions using Aura TES and OMI Observations, J. Geophys.
1126 Res., 120, 3572–3592, doi: 10.1002/2014JD022993.
1127 Huang, M., Carmichael, G. R., Crawford, J. H., Wisthaler, A., Zhan, X., Hain, C. R., Lee, P., and
1128 Guenther, A. B. (2017), Linkages between land initialization of the NASA-Unified WRF v7
1129 and biogenic isoprene emission estimates during the SEAC4RS and DISCOVER-AQ airborne
1130 campaigns, Geosci. Model Dev. Discuss., doi:10.5194/gmd-2017-13, in review.
1131 Inness, A., Blechschmidt, A.-M., Bouarar, I., Chabrillat, S., Crepulja, M., Engelen, R. J., Eskes,
1132 H., Flemming, J., Gaudel, A., Hendrick, F., Huijnen, V., Jones, L., Kapsomenakis, J.,
1133 Katragkou, E., Keppens, A., Langerock, B., de Mazière, M., Melas, D., Parrington, M., Peuch,
1134 V. H., Razinger, M., Richter, A., Schultz, M. G., Suttie, M., Thouret, V., Vrekoussis, M.,
1135 Wagner, A., and Zerefos, C. (2015), Data assimilation of satellite-retrieved ozone, carbon
1136 monoxide and nitrogen dioxide with ECMWF's Composition-IFS, Atmos. Chem. Phys., 15,
1137 5275-5303, doi:10.5194/acp-15-5275-2015.
1138 Jaffe, D.A. (2011), Relationship between surface and free tropospheric ozone in the Western U.S.,
1139 Environ. Sci. Technol., 45, 432–438, doi: 10.1021/es1028102.
1140 Janssens-Maenhout, G., Crippa, M., Guizzardi, D., Dentener, F., Muntean, M., Pouliot, G.,
1141 Keating, T., Zhang, Q., Kurokawa, J., Wankmüller, R., Denier van der Gon, H., Kuenen, J. J.
1142 P., Klimont, Z., Frost, G., Darras, S., Koffi, B., and Li, M. (2015), HTAP_v2.2: a mosaic of
1143 regional and global emission grid maps for 2008 and 2010 to study hemispheric transport of
1144 air pollution, Atmos. Chem. Phys., 15, 11411-11432, doi:10.5194/acp-15-11411-2015.
1145 Jacob, D. J., Logan, J. A., and Murti, P. P. (1999), Effect of rising Asian emissions on surface
1146 ozone in the United States, Geophys. Res. Lett., 26, 2175-2178, doi: 10.1029/1999GL900450.
1147 Jerret, M., R. T. Burnett, C. A. Popo, III, K. Ito, G. Thurston, D. Krewski, Y. Shi, E. Calle, and M.
1148 Thun (2009), Long-Term Ozone Exposure and Mortality, the New England Journal of
1149 Medicine, 360, 1085-1096, doi: 10.1056/NEJMoa0803894.
1150 Kaiser, J. W., Heil, A., Andreae, M. O., Benedetti, A., Chubarova, N., Jones, L., Morcrette, J.-J.,
1151 Razinger, M., Schultz, M. G., Suttie, M., and van der Werf, G. R. (2012), Biomass burning
1152 emissions estimated with a global fire assimilation system based on observed fire radiative
1153 power, Biogeosciences, 9, 527–554, doi:10.5194/bg-9-527-2012.
1154 Kalnay, E., and Co-authors (1996), The NCEP/NCAR 40-Year Reanalysis Project, Bulletin of the
1155 American Meteorological Society, 77, 437–471.
1156 Kim, S.-W., B. C. McDonald, S. Baidar, S. S. Brown, B. Dube, R. A. Ferrare, G. J. Frost, R. A.
1157 Harley, J. S. Holloway, H.-J. Lee, et al. (2016), Modeling the weekly cycle of NO_x and CO
1158 emissions and their impacts on O_3 in the Los Angeles-South Coast Air Basin during the CalNex
1159 2010 field campaign, J. Geophys. Res. Atmos., 121, 1340–1360, doi:10.1002/2015JD024292.
1160 Koffi, B., Dentener, F., Janssens-Maenhout, G., Guizzardi, D., Crippa, M., Diehl, T., Galmarini,
1161 S., and Solazzo, E.: Hemispheric Transport Air Pollution (HTAP): Specification of the HTAP2

experiments – Ensuring harmonized modelling, EUR 28255 EN – Scientific and Technical Research Reports, doi:10.2788/725244, 2016.
Langford, A. O., Brioude, J., Cooper, O.R., Senff, C.J., Alvarez II, R.J., Hardesty, R.M., Johnson, B.J., and Oltmans, S.J. (2011), Stratospheric influence on surface ozone in the Los Angeles area during late spring and early summer of 2010, J. Geophys. Res. Atmos., 117, D00V06, doi: 10.1029/2011JD016766.
Lapina, K., D. K. Henze, J. B. Milford, M. Huang, M. Lin, A. M. Fiore, G. Carmichael, G. G. Pfister, and K. Bowman (2014), Assessment of source contributions to seasonal vegetative exposure to ozone in the U.S., J. Geophys. Res. Atmos., 119, 324–340, doi:10.1002/2013JD020905.
Levelt, P.F., E. Hilsenrath, G.W. Leppelmeier, G.H.J. van den Oord, P.K. Bhartia, J. Tamminen, J.F. de Haan and J.P. Veefkind (2006), Science Objectives of the Ozone Monitoring Instrument, IEEE Transaction on Geoscience and Remote Sensing, 44, 1199-1208.
Li, M., Zhang, Q., Kurokawa, J.-I., Woo, J.-H., He, K., Lu, Z., Ohara, T., Song, Y., Streets, D. G., Carmichael, G. R., Cheng, Y., Hong, C., Huo, H., Jiang, X., Kang, S., Liu, F., Su, H., and Zheng, B. (2017), MIX: a mosaic Asian anthropogenic emission inventory under the international collaboration framework of the MICS-Asia and HTAP, Atmos. Chem. Phys., 17, 935-963, doi:10.5194/acp-17-935-2017.
Lin, M., Holloway, T., Carmichael, G. R., and Fiore, A. M. (2010), Quantifying pollution inflow and outflow over East Asia in spring with regional and global models, Atmos. Chem. Phys., 10, 4221-4239, doi:10.5194/acp-10-4221-2010.
Lin, M., A. M. Fiore, L. W. Horowitz, O. R. Cooper, V. Naik, J. Holloway, B. J. Johnson, A. Middlebrook, S. J. Oltmans, I. B. Pollack, T. B. Ryerson, J. X. Warner, C. Wiedinmyer, J. Wilson, B. Wyman (2012a), Transport of Asian ozone pollution into surface air over the western United States in spring, J. Geophys. Res., 117, D00V07, doi: 10.1029/2011JD016961.
Lin, M., A. Fiore, O. R. R. Cooper, L. W. Horowitz, A. O. O. Langford, H. Levy II, B. J. Johnson, V. Naik, S. J. Oltmans, and C. J. Senff (2012b), Springtime high surface ozone events over the western United States: Quantifying the role of stratospheric intrusions, J. Geophys. Res., 117, D00V22, doi: 10.1029/2012JD018151.
Lin, M., L.W. Horowitz, S. J. Oltmans, A. M. Fiore, S. Fan (2014), Tropospheric ozone trends at Manna Loa Observatory tied to decadal climate variability, Nature Geoscience, 7, 136-143, doi:10.1038/NGEO2066.
Lin, M., L. W. Horowitz, O. R. Cooper, D. Tarasick, S. Conley, L. T. Iraci, B. Johnson, T. Leblanc, I. Petropavlovskikh, and E. L. Yates (2015), Revisiting the evidence of increasing springtime ozone mixing ratios in the free troposphere over western North America, Geophys. Res. Lett., 42, 8719–8728, doi:10.1002/2015GL065311.
Lin, M., Horowitz, L. W., Payton, R., Fiore, A. M., and Tonnesen, G. (2016), US surface ozone trends and extremes from 1980–2014: Quantifying the roles of rising Asian emissions, domestic controls, wildfires, and climate, Atmos. Chem. Phys. Discuss., doi:10.5194/acp-2016-1093, in review.
Liu, F., Q. Zhang, R. J. van der A, B. Zheng, D. Tong, L. Yan, Y. Zheng, and K. He (2016), Recent reduction in NO_x emissions over China: Synthesis of satellite observations and emission inventories, Environ. Res. Lett., 11 (11), 114002, doi: 10.1088/1748-9326/11/11/114002.
Livesey, N.J., M.J. Filipiak, L. Froidevaux, W.G. Read, A. Lambert, M.L. Santee, J.H. Jiang, H.C. Pumphrey, J.W. Waters, R.E. Cofield, D.T. Cuddy, W.H. Daffer, B.J. Drouin, R.A. Fuller, R.F. Jarnot, Y.B. Jiang, B.W. Knosp, Q.B. Li, V.S. Perun, M.J. Schwartz, W.V. Snyder, P.C. Stek,

R.P. Thurstans, P.A. Wagner, M. Avery, E.V. Browell, J-P. Cammas, L.E. Christensen, G.S. Diskin, R-S. Gao, H-J. Jost, M. Loewenstein, J.D. Lopez, P. Nedelec, G.B. Osterman, G.W. Sachse, and C.R. Webster (2008), Validation of Aura Microwave Limb Sounder O3 and CO observations in the upper troposphere and lower stratosphere, J. Geophys. Res. 113, D15S02, doi:10.1029/2007JD008805.

Luecken, D.J., S. Phillips, G. Sarwar, C. Jang, Effects of using the CB05 vs. SAPRC99 vs. CB4 chemical mechanism on model predictions (2008), Ozone and gas-phase photochemical precursor concentrations, Atmos. Environ., 42 (23), 5805-5820, doi: 10.1016/j.atmosenv.2007.08.056.

Maas, R. and P. Grennfelt (eds) (2016), Towards Cleaner Air Scientific Assessment Report 2016. EMEP Steering Body and Working Group on Effects of the Convention on Long-Range Transboundary Air Pollution, Oslo, http://www.unece.org/fileadmin/DAM/env/lrtap/ExecutiveBody/35th_session/CLRTAP_Scientific_Assessment_Report_-_Final_20-5-2016.pdf.

Madronich, S., Flocke, S., Zeng, J., Petropavlovskikh, I., and Lee-Taylor, J. (2002), The Tropospheric Ultra-violet Visible (TUV) model Manual, https://www2.acom.ucar.edu/modeling/tropospheric-ultraviolet-and-visible-tuv-radiation-model.

Mauzerall, D. L. and Wang, X. (2001), Protecting Agricultural Crops from the Effects of Tropospheric Ozone Exposure: Reconciling Science and Standard Setting in the United States, Europe and Asia, Annual Review of Energy and the Environment, 26, 237-268.

McDonald-Buller, E. C., et al. (2011), Establishing policy relevant background (PRB) ozone concentrations in the United States, Environ. Sci. Technol., 45, 9484–9497.

Meijer, E. W., van Velthoven, P. F. J., Brunner, D. W., Huntrieser, H., and Kelder, H. (2001), Improvement and evaluation of the parameterization of nitrogen oxide production by lightning, Phys. Chem. Earth Pt. C, 26, 577–583.

Mesinger, F., DiMego, G., Kalnay, E., Mitchell, K., Shafran, P. C., Ebisuzaki, W., Jovic, D., Woollen, J., Rogers, E., Berbery, E. H., Ek, M. B., Fan, Y., Grumbine, R., Higgins, W., Li, H., Lin, Y., Manikin, G., Parrish, D. and Shi, W. (2006), North American Regional Reanalysis, Bulletin of the American Meteorological Society, 87(3), 343–360, doi: 10.1175/BAMS-87-3-343.

Miyazaki, K., Eskes, H. J., Sudo, K., Takigawa, M., van Weele, M., Boersma, K. F. (2012), Simultaneous assimilation of satellite NO_2, O_3, CO, and HNO_3 data for the analysis of tropospheric chemical composition and emissions, Atmos. Chem. Phys., 12, 9545-9579.

Monks, P. S., Archibald, A. T., Colette, A., Cooper, O., Coyle, M., Derwent, R., Fowler, D., Granier, C., Law, K. S., Mills, G. E., Stevenson, D. S., Tarasova, O., Thouret, V., von Schneidemesser, E., Sommariva, R., Wild, O., and Williams, M. L. (2015), Tropospheric ozone and its precursors from the urban to the global scale from air quality to short-lived climate forcer, Atmos. Chem. Phys., 15, 8889-8973, doi:10.5194/acp-15-8889-2015.

Murray, L. T., D. J. Jacob, J. A. Logan, R. C. Hudman, and W. J. Koshak (2012), Optimized regional and interannual variability of lightning in a global chemical transport model constrained by LIS/OTD satellite data, J. Geophys. Res., 117, D20307, doi:10.1029/2012JD017934.

National Research Council (NRC) (2009), global sources of local pollution-An Assessment of Long-Range Transport of Key Air Pollutants to and from the United States, 35-66, http://books.nap.edu/openbook.php?record_id=12743&page=35.

1254 Neuman, J. A., et al. (2012), Observations of ozone transport from the free troposphere to the Los
1255 Angeles basin, J. Geophys. Res. Atmos., 117, D00V09, doi: 10.1029/2011JD016919.
1256 Oetjen, H., Payne, V. H., Kulawik, S. S., Eldering, A., Worden, J., Edwards, D. P., Francis, G. L.,
1257 Worden, H. M., Clerbaux, C., Hadji-Lazaro, J., and Hurtmans, D. (2014), Extending the
1258 satellite data record of tropospheric ozone profiles from Aura-TES to MetOp-IASI:
1259 characterisation of optimal estimation retrievals, Atmos. Meas. Tech., 7, 4223–4236,
1260 doi:10.5194/amt-7-4223- 2014.
1261 Oetjen, H., Payne, V. H., Neu, J. L., Kulawik, S. S., Edwards, D. P., Eldering, A., Worden, H. M.,
1262 and Worden, J. R. (2016), A joint data record of tropospheric ozone from Aura-TES and
1263 MetOp-IASI, Atmos. Chem. Phys., 16, 10229-10239, doi:10.5194/acp-16-10229-2016.
1264 Ott, L. E., B. N. Duncan, A. M. Thompson, G. Diskin, Z. Fasnacht, A. O. Langford, M. Lin, A. M.
1265 Molod, J. E. Nielsen, S. E. Pusede, et al. (2016), Frequency and impact of summertime
1266 stratospheric intrusions over Maryland during DISCOVER-AQ (2011): New evidence from
1267 NASA's GEOS-5 simulations, J. Geophys. Res. Atmos., 121, 3687–3706,
1268 doi:10.1002/2015JD024052.
1269 Park, R. J., D. J. Jacob, B. D. Field, R. M. Yantosca, and M. Chin (2004), Natural and
1270 transboundary pollution influences on sulfate-nitrate-ammonium aerosols in the United States:
1271 Implications for policy, J. Geophys. Res., 109, D15204, doi:10.1029/2003JD004473.
1272 Parrington, M., D. B. A. Jones, K. W. Bowman, L. W. Horowitz, A. M. Thompson, D. W. Tarasick,
1273 and J. C. Witte (2008), Estimating the summertime tropospheric ozone distribution over North
1274 America through assimilation of observations from the Tropospheric Emission Spectrometer,
1275 J. Geophys. Res., 113, D18307, doi:10.1029/2007JD009341.
1276 Parrington, M., D. B. A. Jones, K. W. Bowman, A. M. Thompson, D. W. Tarasick, J. Merrill, S.
1277 J. Oltmans, T. Leblanc, J. C. Witte, and D. B. Millet (2009), Impact of the assimilation of
1278 ozone from the Tropospheric Emission Spectrometer on surface ozone across North America,
1279 Geophys. Res. Lett., 36, L04802, doi:10.1029/2008GL036935.
1280 Parrish, D. D., D. B. Millet, and A. H. Goldstein (2009), Increasing ozone in marine boundary
1281 layer inflow at the west coasts of North America and Europe, Atmos. Chem. Phys., 9, 1303–
1282 1323, doi:10.5194/acp-9-1303-2009.
1283 Parrish, D. D., Aikin, K. C., Oltmans, S. J., Johnson, B. J., Ives, M., and Sweeny, C. (2010), Impact
1284 of transported background ozone inflow on summertime air quality in a California ozone
1285 exceedance area, Atmos. Chem. Phys., 10, 10093-10109, doi:10.5194/acp-10-10093-2010.
1286 Parrish, D. D., et al. (2012), Long-term changes in lower tropospheric baseline ozone
1287 concentrations at northern mid-latitudes, Atmos. Chem. Phys., 12, 11,485–11,504,
1288 doi:10.5194/acp-12-11485-2012.
1289 Pierce, R. B., et al. (2007), Chemical data assimilation estimates of continental U.S. ozone and
1290 nitrogen budgets during the Intercontinental Chemical Transport Experiment–North America,
1291 J. Geophys. Res., 112, D12S21, doi:10.1029/2006JD007722.
1292 Pierce, R. B., et al. (2009), Impacts of background ozone production on Houston and Dallas, Texas,
1293 air quality during the Second Texas Air Quality Study field mission, J. Geophys. Res., 114,
1294 D00F09, doi:10.1029/2008JD011337.
1295 Pouliot, G., H. A.C. Denier van der Gon, J. Kuenen, J. Zhang, M. D. Moran, P.A. Makar (2015),
1296 Analysis of the emission inventories and model-ready emission datasets of Europe and North
1297 America for phase 2 of the AQMEII project, Atmos. Environ., 115, 345-360.
1298 Qu, Z., D. K. Henze, S. L. Capps, Y. Wang, X. Xu, J. Wang (2016), Monthly top-down NO_x
1299 emissions for China (2005-2012): a hybrid inversion method and trend analysis, submitted.

Quennehen, B., Raut, J.-C., Law, K. S., Daskalakis, N., Ancellet, G., Clerbaux, C., Kim, S.-W., Lund, M. T., Myhre, G., Olivié, D. J. L., Safieddine, S., Skeie, R. B., Thomas, J. L., Tsyro, S., Bazureau, A., Bellouin, N., Hu, M., Kanakidou, M., Klimont, Z., Kupiainen, K., Myriokefalitakis, S., Quaas, J., Rumbold, S. T., Schulz, M., Cherian, R., Shimizu, A., Wang, J., Yoon, S.-C., and Zhu, T. (2016), Multi-model evaluation of short-lived pollutant distributions over east Asia during summer 2008, Atmos. Chem. Phys., 16, 10765-10792, doi:10.5194/acp-16-10765-2016.

Reidmiller, D. R., Fiore, A. M., Jaffe, D. A., Bergmann, D., Cuvelier, C., Dentener, F. J., Duncan, B. N., Folberth, G., Gauss, M., Gong, S., Hess, P., Jonson, J. E., Keating, T., Lupu, A., Marmer, E., Park, R., Schultz, M. G., Shindell, D. T., Szopa, S., Vivanco, M. G., Wild, O., and Zuber, A. (2009), The influence of foreign vs. North American emissions on surface ozone in the US, Atmos. Chem. Phys., 9, 5027-5042, doi:10.5194/acp-9-5027-2009.

Rodgers, C. D. (2000), Inverse Methods for Atmospheric Sounding: Theory and Practice, World Sci., Singapore.

Ryerson, T. B., Andrews, A. E., Angevine, W. M., Bates, T. S., Brock, C. A., Cairns, B., Cohen, R. C., Cooper, O. R., de Gouw, J. A., Fehsenfeld, F. C., Ferrare, R. A., Fischer, M. L., Flagan, R. C., Goldstein, A. H., Hair, J. W., Hardesty, R. M., Hostetler, C. A., Jimenez, J. L., Langford, A. O., McCauley, E., McKeen, S. A., Molina, L. T., Nenes, A., Oltmans, S. J., Parrish, D. D., Pederson, J. R., Pierce, R. B., Prather, K., Quinn, P. K., Seinfeld, J. H., Senff, C. J., Sorooshian, A., Stutz, J., Surratt, J. D., Trainer, M., Volkamer, R., Williams, E. J., Wofsy, S. C. (2013), The 2010 California Research at the Nexus of Air Quality and Climate Change (CalNex) field study, J. Geophys. Res., 118, 5830–5866.

Schere, K. J. Flemming, R. Vautard, C. Chemel, A. Colette, C. Hogrefe, B. Bessagnet, F. Meleux, R. Mathur, S. Roselle, R.-M. Hu, R. S. Sokhi, S. T. Rao, S. Galmarini (2012), Trace gas/aerosol boundary concentrations and their impacts on continental-scale AQMEII modeling domains, Atmos. Environ., 53, 38-50, doi: 10.1016/j.atmosenv.2011.09.043.

Shindell, D. T., G. Faluvegi, D. M. Koch, G. A. Schmidt, N. Unger, and S. E. Bauer (2009), Improved attribution of climate forcing to emissions, Science, 326, 716–718, doi: 10.1126/science.1174760.

Shindell, D. T., et al. (2013), Radiative forcing in the ACCMIP historical and future climate simulations, Atmos. Chem. Phys., 13, 2939–2974, doi:10.5194/acp-13-2939-2013.

Simpson, D., Benedictow, A., Berge, H., Bergström, R., Emberson, L. D., Fagerli, H., Flechard, C. R., Hayman, G. D., Gauss, M., Jonson, J. E., Jenkin, M. E., Nyíri, A., Richter, C., Semeena, V. S., Tsyro, S., Tuovinen, J.-P., Valdebenito, Á., and Wind, P. (2012), The EMEP MSC-W chemical transport model – technical description, Atmos. Chem. Phys., 12, 7825–7865, doi:10.5194/acp-12- 7825-2012.

Sindelarova, K., Granier, C., Bouarar, I., Guenther, A., Tilmes, S., Stavrakou, T., Müller, J.-F., Kuhn, U., Stefani, P., and Knorr, W. (2014), Global data set of biogenic VOC emissions calculated by the MEGAN model over the last 30 years, Atmos. Chem. Phys., 14, 9317–9341, doi:10.5194/acp-14-9317-2014.

Skamarock, W. C., J. B. Klemp, J. Dudhia, D. Gill, D. M. Barker, W. Wang, and J. G. Powers (2008), A description of the Advanced Research WRF version 3 (Available at www.mmm.ucar.edu/wrf/users/docs/arwv3.pdf).

Smith, K. R., Jerrett, M., and Anderson, H. R. et al. (2009), Public health benefits of strategies to reduce greenhouse-gas emissions: health implications of short-lived greenhouse pollutants, Lancet, doi: 10.1016/S0140-6736 (09) 61716-5.

Solazzo, E. R. Bianconi, R. Vautard, K. W. Appel, M. D. Moran, C. Hogrefe, B. Bessagnet, J. Brandt, J. H. Christensen, C. Chemel, I. Coll, H. D. van der Gon, J. Ferreira, R. Forkel, X. V. Francis, G. Grell, P. Grossi, A. B. Hansen, A. Jeričević, L. Kraljević, A. I. Miranda, U. Nopmongcol, G. Pirovano, M. Prank, A. Riccio, K. N. Sartelet, M. Schaap, J. D. Silver, R. S. Sokhi, J. Vira, J. Werhahn, R. Wolke, G. Yarwood, J. Zhang, S.T. Rao, S. Galmarini (2012), Model evaluation and ensemble modelling of surface-level ozone in Europe and North America in the context of AQMEII, Atmos. Environ., 53, 60-74, , doi: 10.1016/j.atmosenv.2012.01.003.

Søvde, O. A., Prather, M. J., Isaksen, I. S. A., Berntsen, T. K., Stordal, F., Zhu, X., Holmes, C. D., and Hsu, J. (2012), The chemical transport model Oslo CTM3, Geosci. Model Dev., 5, 1441–1469, doi:10.5194/gmd-5-1441-2012.

Sudo, K., M. Takahashi, J. Kurokawa, and H. Akimoto (2002), Chaser: A global chemical model of the troposphere, 1. Model description, J. Geophys. Res., 107(D17), 4339, doi:10.1029/2001JD001113.

Stevenson, D. S., et al. (2006), Multimodel ensemble simulations of present-day and near-future tropospheric ozone, J. Geophys. Res., 111, D08301, doi:10.1029/2005JD006338.

Stevenson, D. S., et al. (2013), Tropospheric ozone changes, radiative forcing and attribution to emissions in the Atmospheric Chemistry and Climate Model Intercomparison Project (ACCMIP), Atmos. Chem. Phys., 13, 3063–3085, doi:10.5194/acp-13-3063-2013.

Susaya, J., Kim, K.-H., Shon, Z.-H., Brown R. J. (2013), Demonstration of long-term increases in tropospheric O_3 levels: Causes and potential impacts, Chemosphere, 92, 1520–1528.

Task Force on Hemispheric Transport of Air Pollution (HTAP) (2010), 2010 Final Assessment report, Part A: Ozone and particulate matter, http://www.htap.org/activities/2010_Final_Report/HTAP%202010%20Part%20A%201104 07.pdf.

Tilmes, S., Lamarque, J.-F., Emmons, L. K., Kinnison, D. E., Marsh, D., Garcia, R. R., Smith, A. K., Neely, R. R., Conley, A., Vitt, F., Val Martin, M., Tanimoto, H., Simpson, I., Blake, D. R., and Blake, N. (2016), Representation of the Community Earth System Model (CESM1) CAM4-chem within the Chemistry- Climate Model Initiative (CCMI), Geosci. Model Dev., 9, 1853– 1890, doi:10.5194/gmd-9-1853-2016.

Travis, K. R., Jacob, D. J., Fisher, J. A., Kim, P. S., Marais, E. A., Zhu, L., Yu, K., Miller, C. C., Yantosca, R. M., Sulprizio, M. P., Thompson, A. M., Wennberg, P. O., Crounse, J. D., St. Clair, J. M., Cohen, R. C., Laugher, J. L., Dibb, J. E., Hall, S. R., Ullmann, K., Wolfe, G. M., Pollack, I. B., Peischl, J., Neuman, J. A., and Zhou, X. (2016), Why do models overestimate surface ozone in the Southeast United States?, Atmos. Chem. Phys., 16, 13561-13577, doi:10.5194/acp-16-13561-2016.

United Nations Environment Programme and World Meteorological Organization (2011), Integrated Assessment of Black Carbon and Tropospheric Ozone: Summary for Decision Makers, http://www.unep.org/dewa/Portals/67/pdf/Black_Carbon.pdf.

US EPA (2016a), Implementation of the 2015 Primary Ozone NAAQS: Issues Associated with Background Ozone White Paper for Discussion, https://www.epa.gov/sites/production/files/2016-03/documents/whitepaper-bgo3-final.pdf.

US EPA (2016b), High level summary of background ozone workshop, https://www.epa.gov/sites/production/files/2016-03/documents/bgo3-high-level-summary.pdf.

van der Werf, G. R., Randerson, J. T., Giglio, L., Collatz, G. J., Mu, M., Kasibhatla, P. S., Morton, D. C., DeFries, R. S., Jin, Y., and van Leeuwen, T. T. (2010), Global fire emissions and the contribution of deforestation, savanna, forest, agricultural, and peat fires (1997–2009), Atmos. Chem. Phys., 10, 11707-11735, doi:10.5194/acp-10-11707-2010.

van Noije, T. P. C., Eskes, H. J., Dentener, F. J., Stevenson, D. S., Ellingsen, K., Schultz, M. G., Wild, O., Amann, M., Atherton, C. S., Bergmann, D. J., Bey, I., Boersma, K. F., Butler, T., Cofala, J., Drevet, J., Fiore, A. M., Gauss, M., Hauglustaine, D. A., Horowitz, L. W., Isaksen, I. S. A., Krol, M. C., Lamarque, J.-F., Lawrence, M. G., Martin, R. V., Montanaro, V., Müller, J.-F., Pitari, G., Prather, M. J., Pyle, J. A., Richter, A., Rodriguez, J. M., Savage, N. H., Strahan, S. E., Sudo, K., Szopa, S., and van Roozendael, M. (2006), Multi-model ensemble simulations of tropospheric NO_2 compared with GOME retrievals for the year 2000, Atmos. Chem. Phys., 6, 2943-2979, doi:10.5194/acp-6-2943-2006.

Verstraeten, W. W., K. F. Boersma, J. Zörner, M. A. F. Allaart, K. W. Bowman, and J. R. Worden (2013), Validation of six years of TES tropospheric ozone retrievals with ozonesonde measurements: Implications for spatial patterns and temporal stability in the bias, Atmos. Meas. Tech., 6, 1413–1423.

Verstraeten, W.W., J. L. Neu, J. E. Williams, K. W. Bowman, J. R. Worden, and K. F. Boersma (2015), Rapid increases in tropospheric ozone production and export from China, Nature Geoscience, 8, 690–695, doi:10.1038/ngeo2493.

Wang, H., D. J. Jacob, P. L. Sager, D. G. Streets, R. J. Park, A. B. Gilliland, and A. van Donkelaar (2009), Surface ozone background in the United States: Canadian and Mexican pollution influences, Atmos. Environ., 43(6), 1310–1319, doi:10.1016/j.atmosenv.2008.11.036.

Wang, Y., Konopka, P., Liu, Y., Chen, H., Müller, R., Plöger, F., Riese, M., Cai, Z., and Lü, D. (2012), Tropospheric ozone trend over Beijing from 2002–2010: ozonesonde measurements and modeling analysis, Atmos. Chem. Phys., 12, 8389-8399, doi:10.5194/acp-12-8389-2012.

Warneke, C., J. A. deGouw, J. S. Holloway, J. Peischl, T. B. Ryerson, E. Atlas, D. Blake, M. Trainer, and D. D. Parrish (2012), Multiyear trends in volatile organic compounds in Los Angeles, California: Five decades of decreasing emissions, J. Geophys. Res., 117, D00V17, doi:10.1029/2012JD017899.

Warner, J. X., McCourt Comer, M., Barnet, C. D., McMillan, W. W., Wolf, W., Maddy, E., and Sachse, G. (2007), A comparison of satellite tropospheric carbon monoxide measurements from AIRS and MOPITT during INTEX-A, J. Geophys. Res., 112, D12S17, doi:10.1029/2006JD007925, 2007.

Wiedinmyer, C., Akagi, S. K., Yokelson, R. J., Emmons, L. K., Al-Saadi, J. A., Orlando, J. J., and Soja, A. J. (2011), The Fire INventory from NCAR (FINN): a high resolution global model to estimate the emissions from open burning, Geosci. Model Dev., 4, 625-641, doi:10.5194/gmd-4-625-2011.

Wigder, N.L., Jaffe, D.A., Herron-Thorpe, F.L., and Vaughan, J.K. (2013), Influence of daily variations in baseline ozone on urban air quality in the United States Pacific Northwest, J. Geophys. Res., 118, 3343–3354, doi: 10.1029/2012JD018738.

Wild, O., Fiore, A. M., Shindell, D. T., Doherty, R. M., Collins, W. J., Dentener, F. J., Schultz, M. G., Gong, S., MacKenzie, I. A., Zeng, G., Hess, P., Duncan, B. N., Bergmann, D. J., Szopa, S., Jonson, J. E., Keating, T. J., and Zuber, A. (2012), Modelling future changes in surface ozone: a parameterized approach, Atmos. Chem. Phys., 12, 2037-2054, doi:10.5194/acp-12-2037-2012.

Wu, S., B. N. Duncan, D. J. Jacob, A. M. Fiore, and O. Wild (2009), Chemical nonlinearities in relating intercontinental ozone pollution to anthropogenic emissions, Geophys. Res. Lett., 36, L05806, doi:10.1029/2008GL036607.

Yarwood, G., Rao, S., Yocke, M., and Whitten, G. (2005), Updates to the carbon bond chemical mechanism: CB05. Final report to the US EPA, EPA Report Number: RT-0400675.

Zhang, L., Jacob, D. J., Boersma, K. F., Jaffe, D. A., Olson, J. R., Bowman, K. W., Worden, J. R., Thompson, A. M., Avery, M. A., Cohen, R. C., Dibb, J. E., Flock, F. M., Fuelberg, H. E., Huey, L. G., McMillan, W. W., Singh, H. B., and Weinheimer, A. J. (2008), Transpacific transport of ozone pollution and the effect of recent Asian emission increases on air quality in North America: an integrated analysis using satellite, aircraft, ozonesonde, and surface observations, Atmos. Chem. Phys., 8, 6117-6136, doi:10.5194/acp-8-6117-2008.

Zhang, L., Jacob, D. J., Kopacz, M., Henze, D. K., Singh, K., and Jaffe, D. A. (2009), Intercontinental source attribution of ozone pollution at western U.S. sites using an adjoint method, Geophys. Res. Lett., 36, L11810, doi: 10.1029/2009GL037950.

Zhang, L., D. J. Jacob, N. V. Downey, D. A. Wood, D. Blewitt, C. C. Carouge, A. van Donkelaar, D. B. A. Jones, L. T. Murray, and Y. Wang (2011), Improved estimate of the policy-relevant background ozone in the United States using the GEOS-Chem global model with 1/2°×2/3° horizontal resolution over North America, Atmos. Environ., 45, 6769–6776, doi: 10.1016/j.atmosenv.2011.07.054.

Zhang, Q., Yuan, B., Shao, M., Wang, X., Lu, S., Lu, K., Wang, M., Chen, L., Chang, C.-C., and Liu, S. C. (2014), Variations of ground-level O_3 and its precursors in Beijing in summertime between 2005 and 2011, Atmos. Chem. Phys., 14, 6089-6101, doi:10.5194/acp-14-6089-2014.

Zhang, Y., Y. Chen, G. Sarwar, and K. Schere (2012), Impact of gas-phase mechanisms on Weather Research Forecasting Model with Chemistry (WRF/Chem) predictions: Mechanism implementation and comparative evaluation, J. Geophys. Res., 117, D01301, doi:10.1029/2011JD015775.

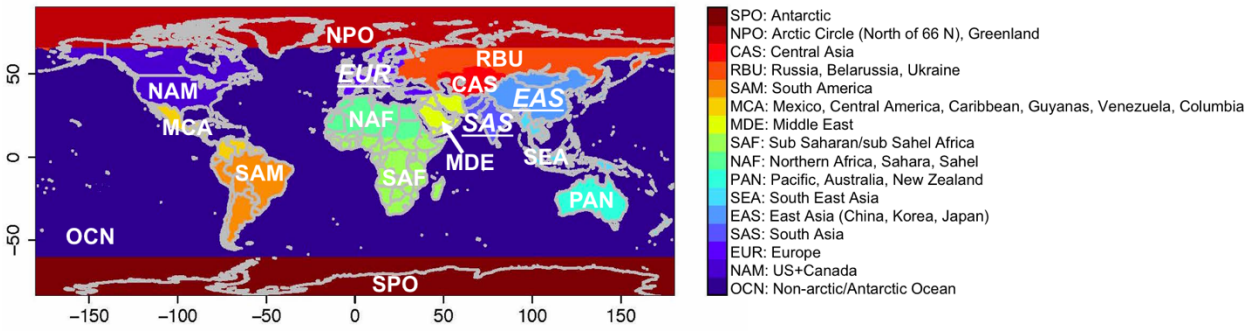

Figure 1. Definitions of the 16 source regions used in HTAP2 SR relationship study (More details in Koffi et al., 2016). The map is plotted based on data on a 0.1°×0.1° resolution grid. We focus in this study on the impact of anthropogenic pollution from selected non-North American source regions (i.e., EAS, SAS, and EUR), whose names are underlined and in italic.

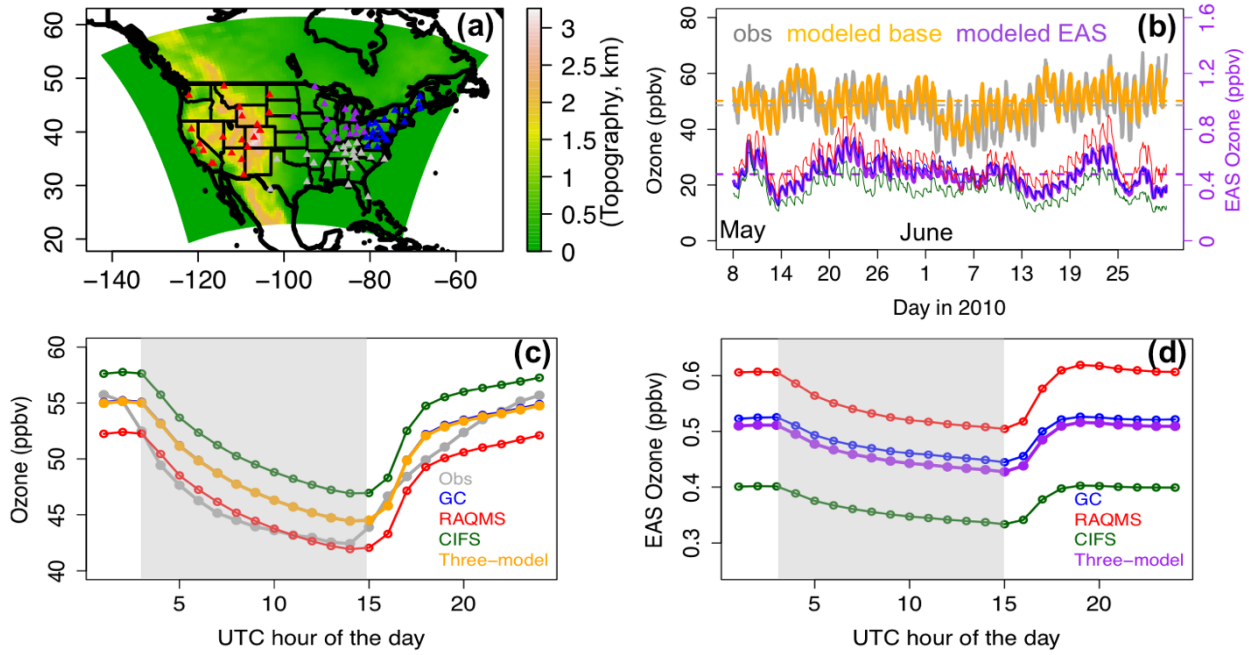

Figure 2. (a) The 60 km STEM NAM domain, colored by the model topography. The CASTNET sites used in the STEM base O_3 evaluation are marked as triangles in different colors that identify the subregions they belong to (red: western US; grey: southern US; purple: Midwest; blue: northeastern US). **(b)** Evaluation of the STEM modeled (averaged from the three base simulations using the GEOS-Chem, ECMWF C-IFS, and RAQMS base runs as the chemical boundary conditions) hourly O_3 at the western US (i.e., EPA regions 8, 9, and 10) CASTNET sites. Observations, modeled base O_3 and the modeled R(O_3, EAS, 20%) are in grey, orange, and purple lines, respectively. The horizontal dashed lines indicate the period mean values. The R(O_3, EAS, 20%) values from STEM calculations using three different chemical boundary conditions are shown separately in thin lines (blue: GEOS-Chem; red: RAQMS; green: C-IFS). The period-mean diurnal variability of the STEM modeled **(c)** base and **(d)** R(O_3, EAS, 20%) at the western US CASTNET sites. The STEM calculations using three different chemical boundary conditions are shown separately as well as averagely. Light grey-shaded areas indicate the local standard nighttime (from 6/7 pm to 7/8 am).

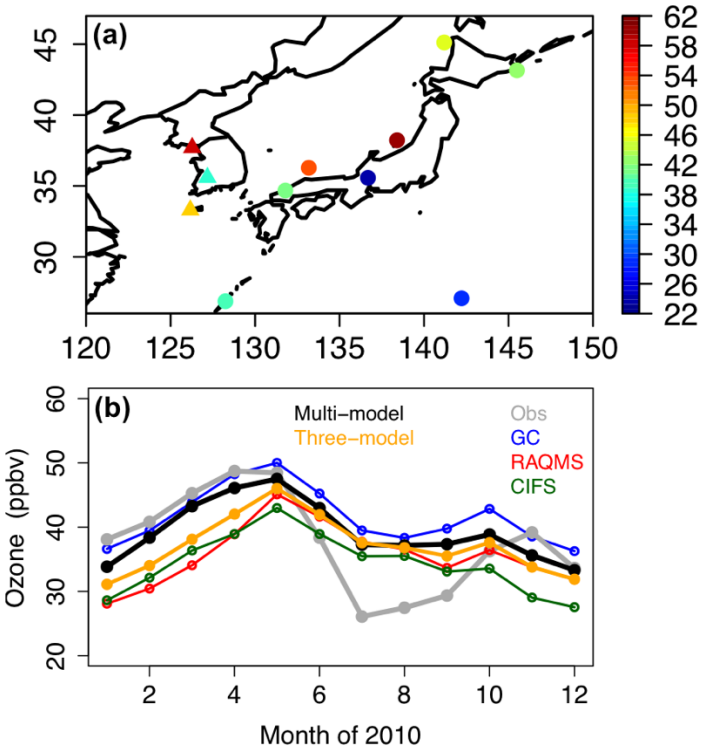

Figure 3. (a) May-June 2010 period mean surface O_3 observations in ppbv at eight Japanese (filled circles) and three Korean (filled triangles) EANET sites. **(b)** Observed and modeled monthly-mean surface O_3 in 2010 at all eleven EANET sites. The "Multi-model" and "Three-model" in the legend indicate the mean values of all eight global models and only of the three boundary condition models, respectively.

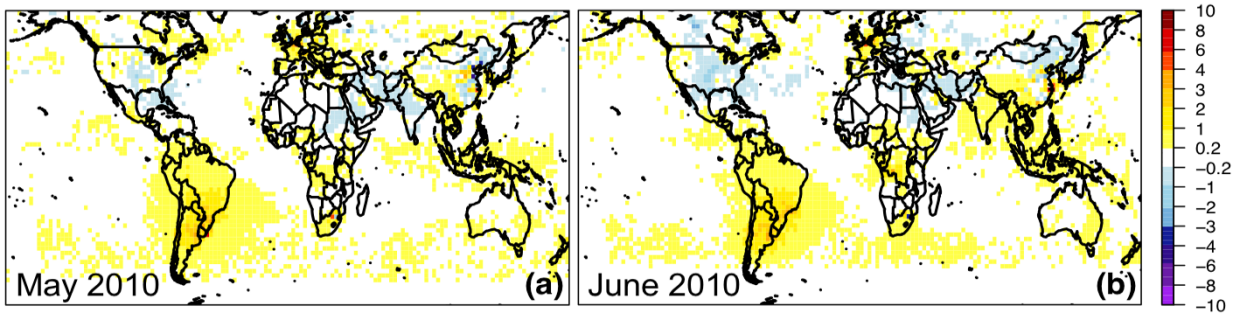

Figure 4. Evaluation of the GEOS-Chem adjoint base NO_2 product (recorded at near the satellite overpassing time) with the OMI NO_2 columns. The differences between OMI and GEOS-Chem (OMI-modeled) tropospheric NO_2 columns ($\times 10^{15}$ molec./cm^2) are shown for **(a)** May and **(b)** June 2010. Details of the comparison are included in Section 2.3.2.

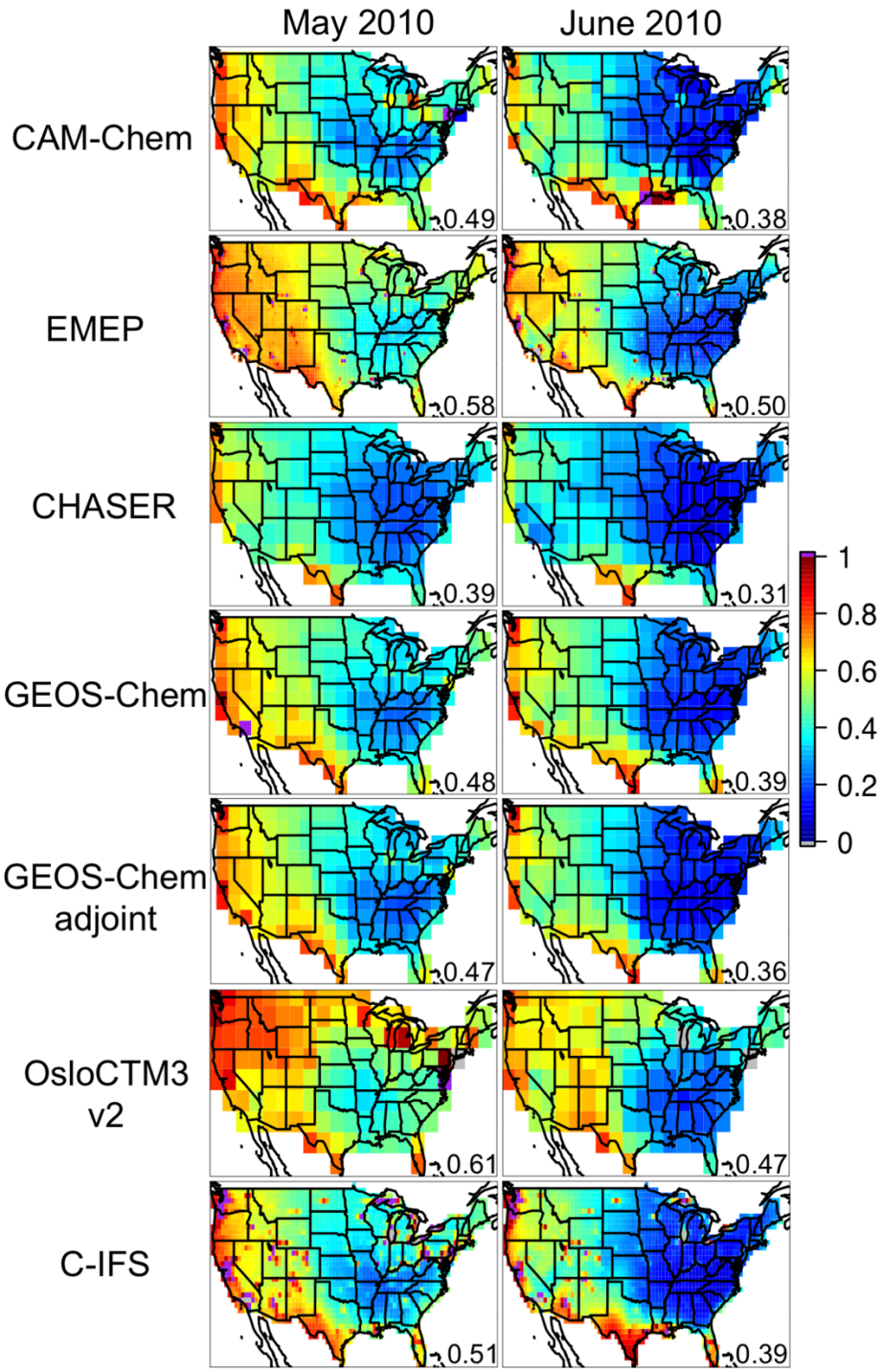

Figure 5. The RERER maps in May (left) and June (right) 2010 over the continental US, calculated based on the monthly mean O_3 from multiple global models' base and emission sensitivity simulations. The RERER metric (unitless) was defined in eq. (2) in the text. Values larger than 1 and smaller than 0 are shown in purple and grey, respectively. The US (including continental US as well as Hawaii which is not shown in the plots) mean values are indicated for each panel at the lower right corner. All models show declining RERER values from May to June, and the 7-model mean RERER values for May and June 2010 are ~0.5 and ~0.4, respectively.

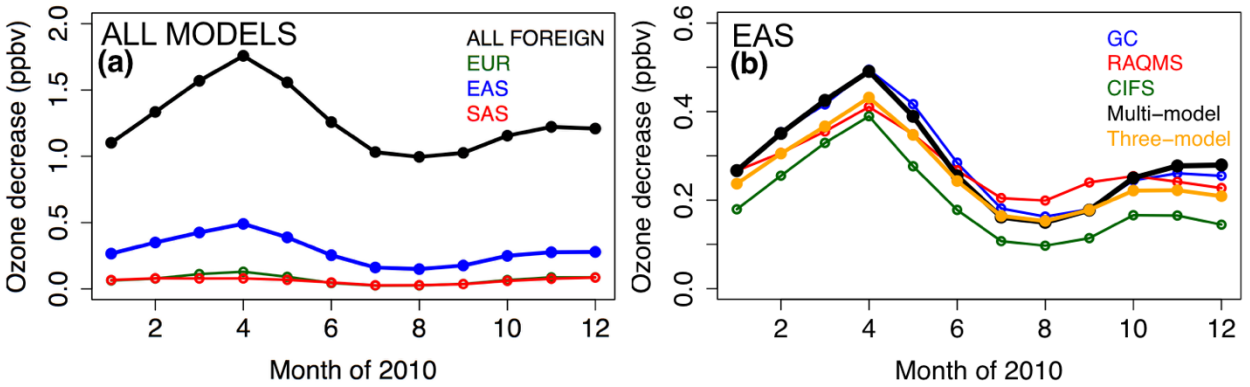

Figure 6. (a) North American (130-65°W; 20-50°N) mean O_3 sensitivity to 20% anthropogenic emission reductions in various non-North American regions, averaged from multiple (six-eight, see details in text) global models. **(b)** North American surface R(O_3, EAS, 20%) values, as estimated by single (the three STEM boundary condition models) or multi- global model means. The "Multi-model" and "Three-model" in the legend indicate the mean sensitivities of all eight global models and only of the three boundary condition models, respectively.

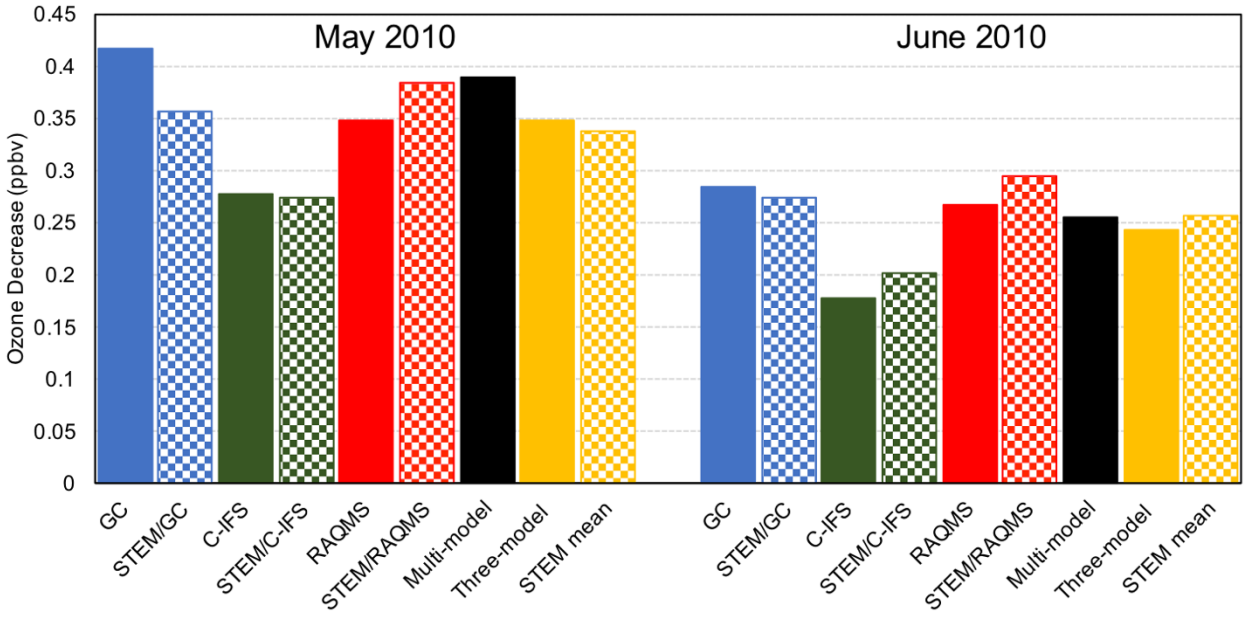

Figure 7. Monthly-mean North American (130-65°W; 20-50°N) surface R(O_3, EAS, 20%) values from multiple global and regional model simulations for May (left) and June (right) 2010. STEM model mean values were calculated from its hourly output from 8 May and on. The "Multi-model" and "Three-model" in the legend indicate the mean sensitivities of all eight global models and only of the three boundary condition models, respectively.

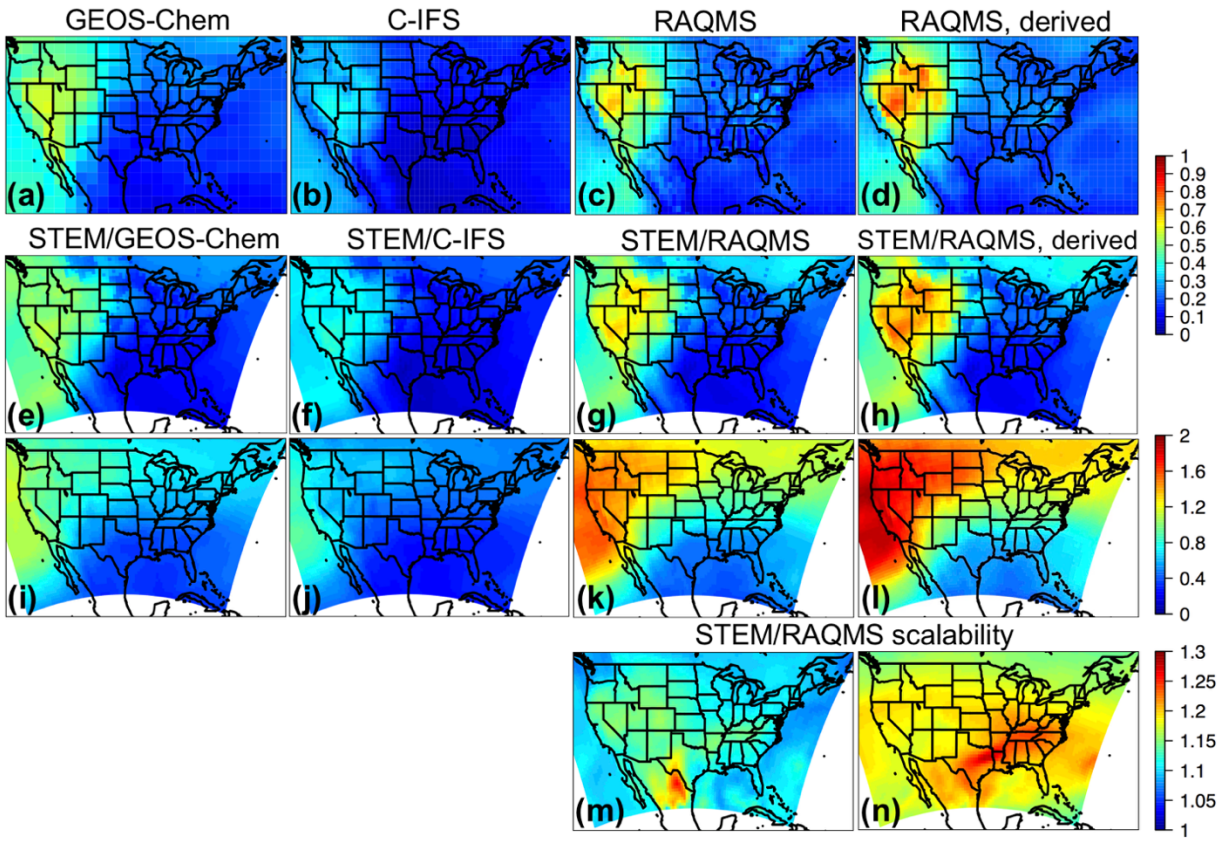

Figure 8. The monthly-mean R(O_3, EAS, 20%) in June 2010 for: **(a-d)** surface O_3 (ppbv) from the three boundary condition models, **(e-h)** STEM surface O_3 (ppbv), and **(i-l)** STEM column O_3 ($\times 10^{16}$ molecules/cm^2). R(O_3, EAS, 20%) values from the simulations associated with GEOS-Chem, ECMWF C-IFS, and RAQMS are shown in **(a;e;i)**, **(b;f;j)** and **(c;g;k)**, respectively. **(d;h;l)** show 1/5 of the R(O_3, EAS, 100%) from the simulations related to RAQMS. STEM/RAQMS-based "Scalability" S_{O3} (eq. (3)) values over the NAM are shown for **(m)** surface and **(n)** column O_3.

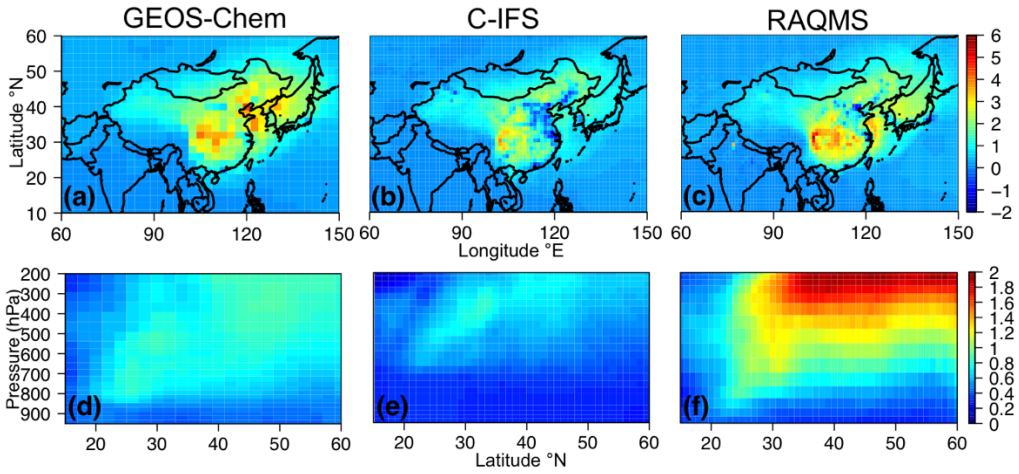

Figure 9. The monthly-mean R(O_3, EAS, 20%) in ppbv in June 2010 from the three boundary condition models at the source and near the receptor regions: **(a-c)** surface O_3 in the East Asia; and **(d)** O_x (GEOS-Chem) or **(e-f)** O_3 (ECMWF C-IFS and RAQMS) along the cross section of 135°W (near the west boundary of the STEM model domain as defined in Figure 2a).

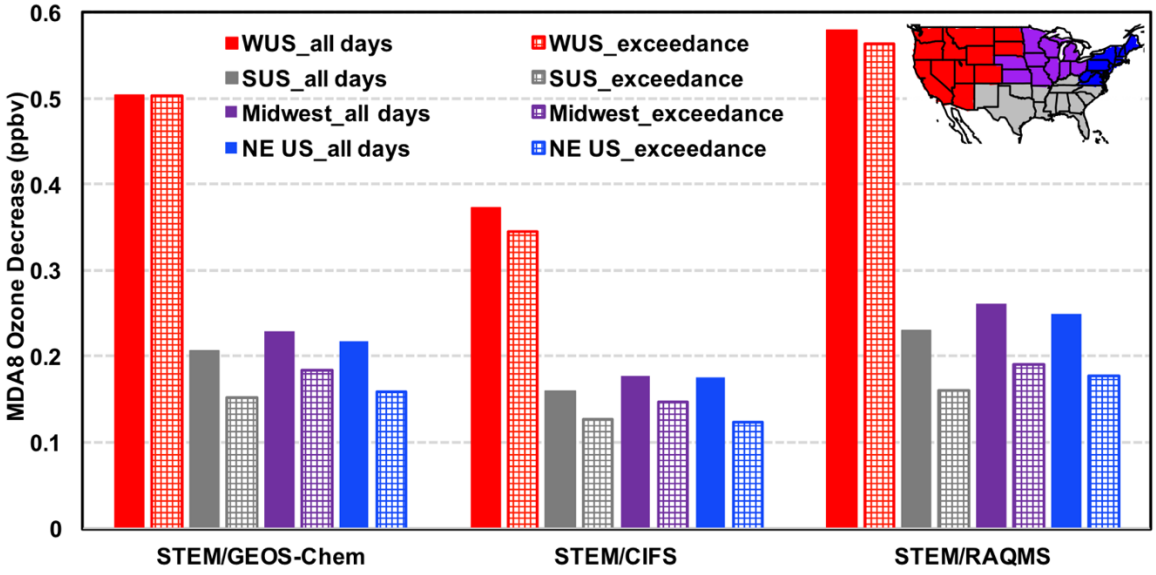

Figure 10. STEM R(MDA8, EAS, 20%) for May-June 2010 in four US subregions (defined in the inset panel, also consistent with the definitions in Figures 2/S4 and Tables 2-3), averaged on all days (bars with solid fill) and only on the days when the simulated total MDA8 O_3 concentrations were over 70 ppbv (bars with grid pattern fill). The results from the STEM runs using GEOS-Chem, ECMWF C-IFS and RAQMS boundary conditions are shown separately.

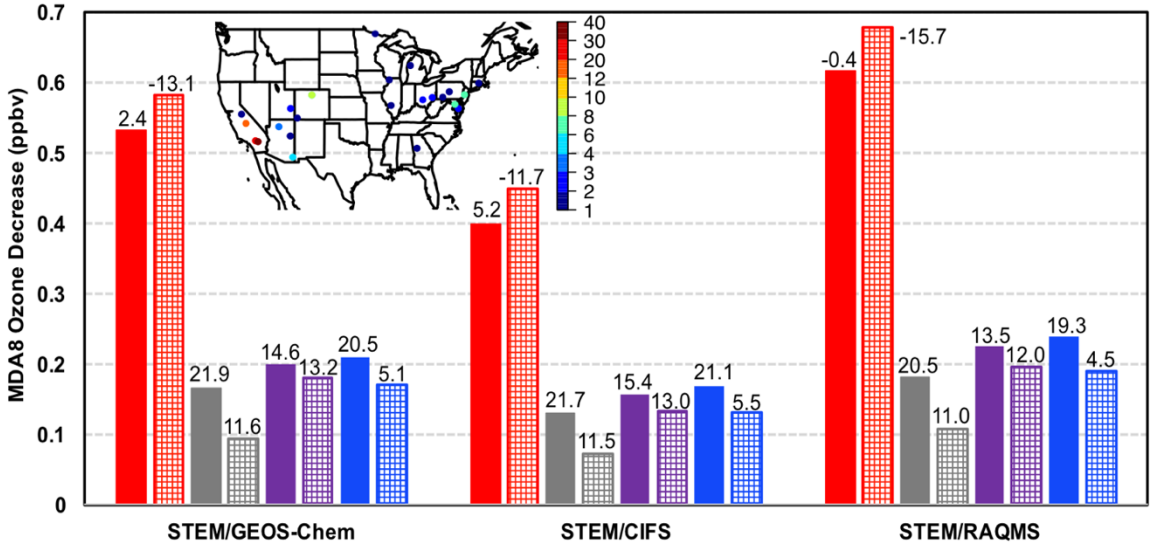

Figure 11. STEM R(MDA8, EAS, 20%) for May-June 2010 at the CASTNET sites in four US subregions (same definition as in Figure 10 inset), averaged on all days (bars with solid fill) and only on the days when the observed MDA8 O_3 concentrations were over 70 ppbv (bars with grid pattern fill). The results from the STEM runs using GEOS-Chem, ECMWF C-IFS and RAQMS boundary conditions are shown separately. Biases for the corresponding model base runs are shown above the bar plots. Inset shows at various CASTNET sites the number of days when the observed MDA8 O_3 concentrations were over 70 ppbv.

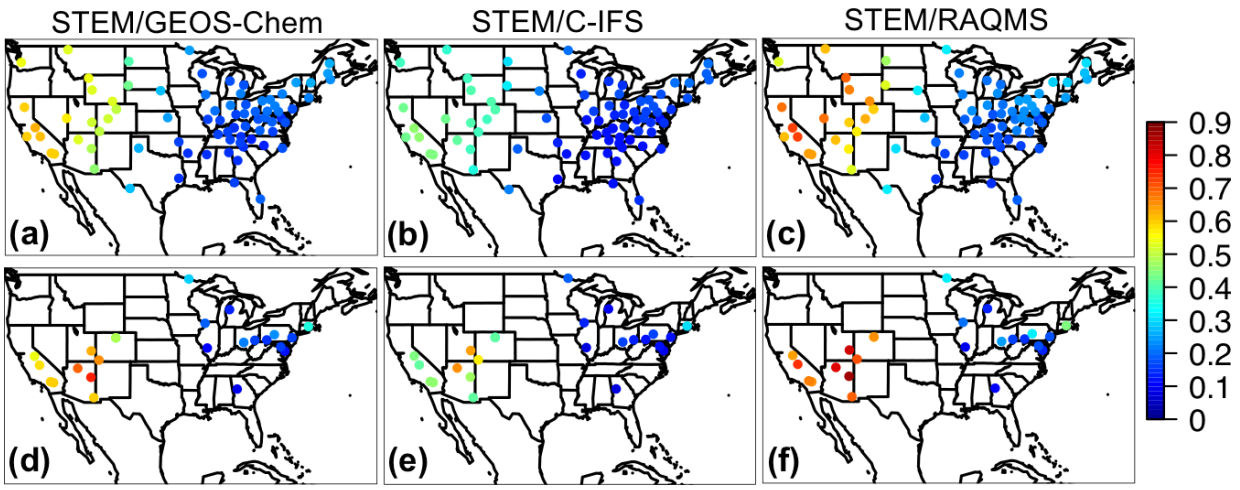

Figure 12. STEM R(MDA8, EAS, 20%) in ppbv for May-June 2010 at the CASTNET sites on **(a-c)** all days and **(d-f)** the days when the observed MDA8 O_3 concentrations were over 70 ppbv. The results from the STEM runs using **(a;d)** GEOS-Chem, **(b;e)** ECMWF C-IFS and **(c;f)** RAQMS boundary conditions are shown separately.

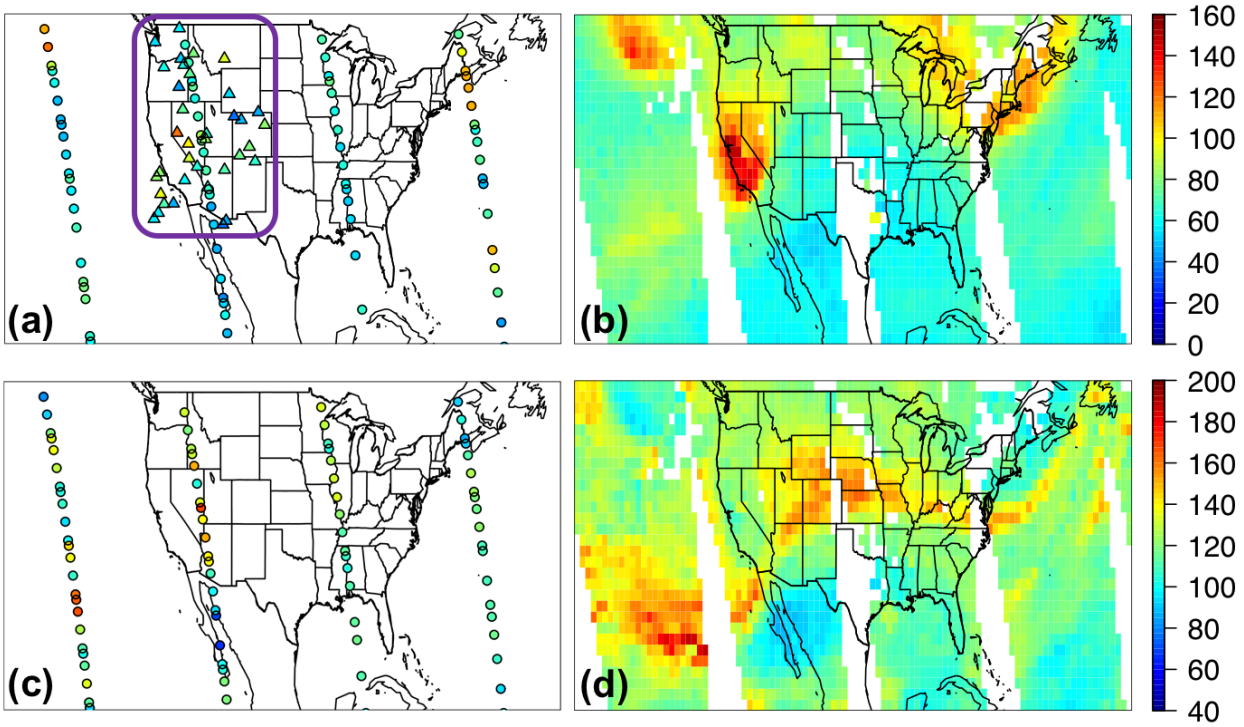

Figure 13. Case study of 9 May 2010: **(a-b)** Ozone (ppbv) and **(c-d)** CO (ppbv) at ~500 hPa from the L2 **(a;c)** TES retrievals (circles) and **(b;d)** L3 AIRS products at early afternoon local time. The L2 IASI O_3 (ppbv) at ~500 hPa retrieved using the TES algorithm (details in Section 2.3.2) at the mid- morning local times is shown on panel (b) as triangles. The O_3 profiles within the purple box in panel (a) were used in the model evaluation shown in Figure 14.

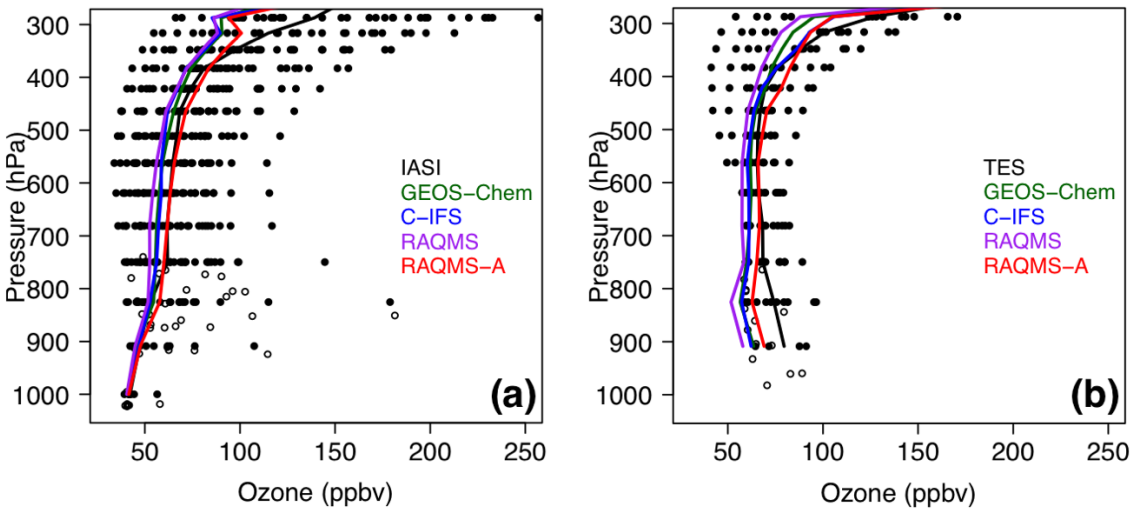

Figure 14. Case study of 9 May 2010: The comparisons between **(a)** IASI and **(b)** TES O_3 in the western US with the simulated O_3 in the STEM runs using the GEOS-Chem (green), C-IFS (blue), RAQMS (purple), and assimilated RAQMS (red) boundary conditions. The O_3 profiles within the purple box in Figure 10a were used in the evaluation. Observation operators were applied in the comparisons (details in Section 2.3.2). Solid and open dots are TES/IASI data at the TES retrieval reporting levels and at the variable surface pressure levels, respectively. Solid lines are median O_3 profiles from the satellite observations and the different STEM simulations, calculated only on the TES retrieval reporting levels.

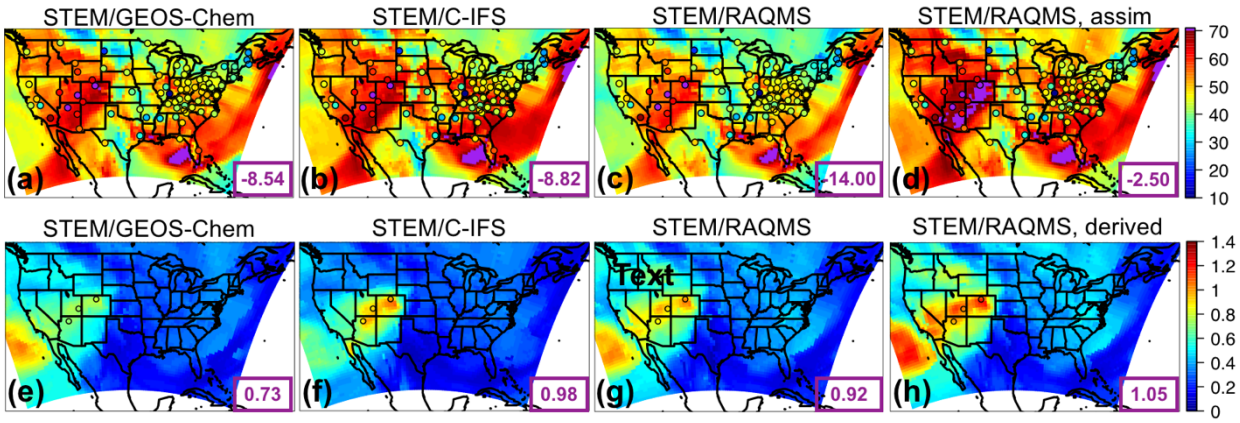

Figure 15. Case study of 9 May 2010: **(a-d)** Surface MDA8 total O_3 and **(e-h)** surface R(MDA8, EAS, 20%) from the STEM simulations using the (**a;e**) GEOS-Chem, **(b;f)** ECMWF C-IFS, and **(c;g)** RAQMS free run as the boundary conditions. **(d)** Surface MDA8 total O_3 in a STEM base simulation using the RAQMS assimilation run as the boundary conditions. CASTNET observations are overlaid in filled circles in panels (a-d). **(h)** 1/5 of the surface R(MDA8, EAS, 100%) from STEM/RAQMS simulations. The conditions at ~400-500 hPa are shown in Figure S5. Purple numbers at the lower right corners of **(a-d)** and **(e-h)** are mean model biases and mean R(MDA8, EAS, 20%) values in ppbv at the three mountain sites (Grand Canyon NP, AZ; Canyonlands NP, UT; and Rocky Mountain NP, CO) where O_3 exceedances were observed on this day. The locations of these sites are shown in panel **(e-h)** as open circles.

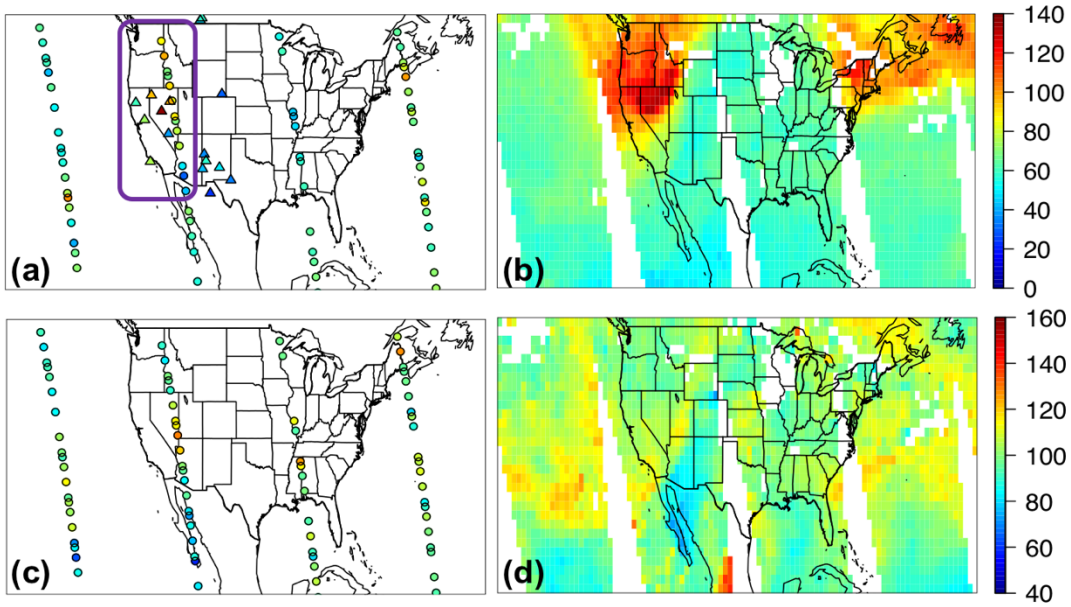

Figure 16. Same as Figure 13, but for a case study of 10 June 2010.

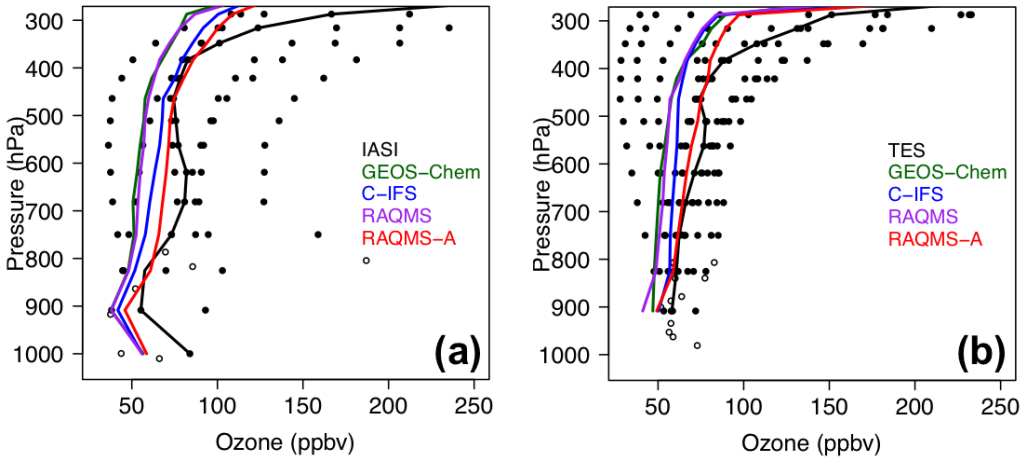

Figure 17. Same as Figure 14, but for a case study of 10 June 2010.

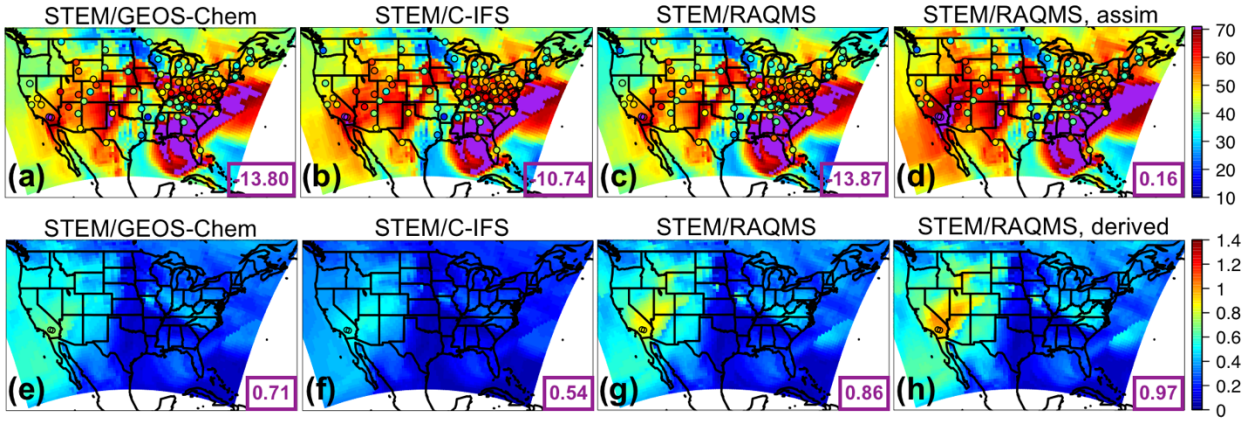

Figure 18. Same as Figure 15, but for a case study of 10 June 2010. The CASTNET sites with O_3 exceedances on this day are Converse Station and Joshua Tree NP in southern California.

Table 1a. HTAP2 base and sensitivity simulations by various global models. The STEM boundary condition models are highlighted in bold.

Global model, Resolution: lon×lat×vertical layer, (References)	BASE	EASALL (-20%)	EASALL (-100%)	GLOALL (-20%)	NAMALL (-20%)	EURALL (-20%)	SASALL (-20%)
CAM-Chem, 2.5°×1.9°×56 (Tilmes et al., 2016)	✓	✓		✓	✓	✓	✓
CHASER T42, ~2.8°×2.8°×32 (Sudo et al., 2002)	✓	✓		✓	✓	✓	✓
EMEP rv48, 0.5°×0.5°×20 (Simpson et al., 2012)	✓	✓		✓	✓	✓	✓
SNU GEOS-Chem v9-01-03, 2°×2.5°×47 (Park et al., 2004; http://iek8wikis.iek.fz-juelich.de/HTAPWiki/WP2.3?action=AttachFile&do=view&target=_README_GEOS-Chem.pdf)	✓	✓		✓	✓		
CU-Boulder GEOS-Chem adjoint v35f, 2°×2.5°×47 (Henze et al., 2007)	✓	✓		✓	✓	✓	✓
RAQMS, 1°×1°×35, free running (Pierce et al., 2007, 2009)	✓	✓	✓				
RAQMS, 1°×1°×35, with satellite assimilation (Pierce et al., 2007, 2009)	✓						
OsloCTM3 v2, ~2.8°×2.8°×60 (Søvde et al., 2012)	✓	✓		✓	✓	✓	✓
ECMWF C-IFS, ~0.7°×0.7°×54/**1.125°×1.125°×54, as the STEM chemical boundary conditions** (Flemming et al., 2015)	✓	✓		✓	✓	✓	✓

Acronyms:
CAM-Chem: Community Atmosphere Model with Chemistry
C-IFS: Composition-Integrated Forecasting System
ECMWF: European Center for Medium range Weather Forecasting
EMEP: European Monitoring and Evaluation Programme
GEOS-Chem: Goddard Earth Observing System with Chemistry
RAQMS: Realtime Air Quality Modeling System
SNU: Seoul National University

Table 1b. STEM regional simulations for HTAP2

Boundary condition model, Resolution: lon×lat×vertical layer	BASE	EASALL (-20%)	EASALL (-100%)
SNU GEOS-Chem v9-01-03, 2°×2.5°×47	✓	✓	
RAQMS, 1°×1°×35, free running	✓	✓	✓
RAQMS, 1°×1°×35, with satellite assimilation	✓		
ECMWF C-IFS, 1.125°×1.125°×54	✓	✓	

Table 1c. STEM and its boundary condition models' key inputs and chemical mechanisms, with references. More details on the models can be found in Table 1a and the text.

Model	Meteorology	Biogenic VOCs; NO_x	Lightning	Biomass Burning	Chemical Mechanism
GEOS-Chem	GEOS-5	MEGAN v2.1 (Guenther et al., 2012); Wang et al., 2009	based on GEOS-5 deep convective cloud top heights and climatological observations (Murray et al., 2012)	GFED v3.0 (van der Werf et al., 2010)	GEOS-Chem standard NO_x-O_x-hydrocarbon-aerosol (http://acmg.seas.harvard.edu/geos/doc/archive/man.v9-01-03/appendix_1.html)
RAQMS	Online (Pierce et al., 2007)				CB-IV (Gery et al., 1989) with adjustments
ECMWF C-IFS	IFS	MEGAN-MACC, (Sindelarova et al., 2014); POET database for 2000 (Granier et al., 2005)	based on IFS convective precipitation (Meijer et al., 2001)	GFAS v1.0 (Kaiser et al., 2012)	CB05 (Yarwood et al., 2005)
STEM	WRF-ARW v3.3.1	WRF-MEGAN v2.1	based on scaled WRF convective precipitation	FINN v1.0 (Wiedinmyer et al., 2011)	SAPRC99 (Carter, 2000)

Acronyms:
CB: Carbon Bond
FINN: Fire INventory from NCAR
GFAS: Global Fire Assimilation System
GFED: Global Fire Emissions Database
IFS: Integrated Forecasting System
MACC: Monitoring Atmospheric Composition and Climate
MEGAN: Model of Emissions of Gases and Aerosols from Nature
POET: Precursors of Ozone and their Effects in the Troposphere
WRF-ARW: Advanced Research Weather Research and Forecasting Model

Table 2a. Evaluation of the period mean (1 May-30 June, 2010) multi- global model free simulations against the CASTNET observations, only at the sites where 95% of the hourly O_3 observations are available. Evaluation of the individual models is summarized in Table 2b.

Subregion	US EPA regions contained	Number of sites	Mean bias (ppbv)		RMSE (ppbv)	
			3 BC[a] models	8 global models	3 BC models	8 global models
Western US	8, 9, 10	19	-5.68	-2.52	10.37	7.05
Southern US	4, 6	18	11.61	10.24	13.62	11.96
Midwest	5, 7	13	8.03	7.66	9.16	8.67
Northeast	1, 2, 3	17	9.55	10.63	10.28	11.24
All	1-10	67	5.49	6.22	11.11	9.96

[a]BC: Boundary Conditions

Table 2b. Evaluation of the period mean (May-June 2010) global model free simulations against the EANET and CASTNET observations. The STEM boundary condition models are highlighted in bold.

Network	Number of sites	RMSE (ppbv)							
		CAM-Chem	EMEP	CHASER	**SNU GEOS-Chem**	GEOS-Chem adjoint	**RAQMS**	OsloCTM3 v2	**C-IFS**
CASTNET	67	13.30	11.61	15.43	**15.55**	13.48	**9.32**	11.05	**11.00**
EANET	11	10.38	9.96	11.39	**9.18**	11.04	**8.60**	12.97	**10.86**

Table 2c. Evaluation of the period mean (May-June 2010) multi- global model free simulations against the EANET observations in Japan and Korea. Evaluation of the individual models is summarized in Table 2b.

Country	Number of sites	Mean bias (ppbv)		RMSE (ppbv)	
		3 BC[a] models	8 global models	3 BC models	8 global models
Japan	8	0.36	1.01	8.77	9.25
Korea	3	1.14	3.98	8.37	10.51
All	11	0.57	1.82	8.66	9.61

[a]BC: Boundary Conditions

Table 3a. Evaluation of the hourly STEM simulated total O_3 (averaged from the three base simulations that used the different free-running boundary conditions) against the CASTNET surface observations for 8 May-30 June, 2010. The subregional mean R(O_3, EAS, 100%) and its correlation coefficient with the observed O_3 are also shown.

Subregion	US EPA regions contained	Number of sites	Mean elevation (km): actual/model	Mean bias (ppbv)	RMSE (ppbv)	Correlation (model base; obs)	Correlation (obs; modeled EAS)	Mean EAS sensitivity (ppbv)
Western US	8, 9, 10	22	1.75/ 1.71	1.60	4.86	0.76	0.34	0.48
Southern US	4, 6	22	0.38/ 0.31	20.33	22.13	0.58	0.27	0.15
Midwest	5, 7	16	0.29/ 0.28	15.64	17.97	0.70	0.15	0.17
Northeast	1, 2, 3	20	0.36/ 0.26	20.94	24.16	0.47	0.17	0.21
All	1-10	80	0.73/ 0.68	16.17	18.30	0.66	0.13	0.20

Table 3b. Evaluation of the hourly STEM simulated total O_3 (separately for three base simulations that used the different free-running boundary conditions) against the CASTNET surface observations for 8 May-30 June, 2010.

Subregion	US EPA regions contained	Number of sites	Mean bias (ppbv)/RMSE (ppbv)/Correlation (model base; obs)		
			SNU GEOS-Chem	C-IFS	RAQMS
Western US	8, 9, 10	22	1.68/4.83/0.77	4.16/6.63/0.70	-1.03/4.81/0.76
Southern US	4, 6	22	21.18/22.94/0.57	20.34/22.07/0.60	19.48/21.45/0.56
Midwest	5, 7	16	15.77/18.17/0.70	16.41/18.46/0.72	14.73/17.35/0.69
Northeast	1, 2, 3	20	21.25/24.36/0.47	21.86/24.80/0.48	19.71/23.40/0.45
All	1-10	80	16.57/18.62/0.66	16.89/18.84/0.67	15.03/17.52/0.64

Table 4. The ranges and standard deviations (ppbv, separated by ";") of R(O_3, *source region*, 20%) by 6-8 global models (defined in eq. (1a-d)), summarized by months in 2010. The monthly multi-model mean values are shown in Figures 5-6.

Month/ Source region	All Foreign/ Non-NAM (ppbv)	EUR (ppbv)	EAS (ppbv)	SAS (ppbv)
Jan	0.38-1.69; 0.41	0.002-0.12; 0.05	0.02-0.72; 0.24	0.001-0.11; 0.04
Feb	0.92-2.07; 0.37	0.02-0.15; 0.05	0.16-0.91; 0.28	0.02-0.12; 0.04
Mar	1.30-2.37; 0.38	0.07-0.21; 0.06	0.24-1.03; 0.30	0.03-0.12; 0.03
Apr	1.42-2.46; 0.33	0.09-0.23; 0.05	0.33-1.07; 0.28	0.04-0.12; 0.03
May	1.24-1.91; 0.21	0.06-0.17; 0.04	0.24-0.75; 0.19	0.05-0.11; 0.02
Jun	1.03-1.41; 0.13	0.03-0.07; 0.02	0.14-0.39; 0.09	0.04-0.07; 0.01
Jul	0.86-1.18; 0.13	0.02-0.04; 0.01	0.08-0.22; 0.06	0.01-0.04; 0.01
Aug	0.80-1.19; 0.13	0.01-0.04; 0.01	0.07-0.20; 0.05	0.02-0.04; 0.01
Sep	0.85-1.18; 0.13	0.03-0.05; 0.01	0.10-0.25; 0.06	0.02-0.06; 0.01
Oct	0.96-1.31; 0.14	0.04-0.10; 0.02	0.17-0.42; 0.09	0.03-0.08; 0.02
Nov	0.90-1.48; 0.19	0.05-0.15; 0.04	0.17-0.54; 0.14	0.04-0.10; 0.02
Dec	0.73-1.67; 0.29	0.03-0.18; 0.05	0.14-0.66; 0.19	0.04-0.12; 0.03